

Initial data for general relativistic simulations of multiple electrically charged black holes with linear and angular momenta

Gabriele Bozzola*

Department of Astronomy, University of Arizona, Tucson, Arizona 85721, USA

Vasileios Paschalidis†

Departments of Astronomy and Physics, University of Arizona, Tucson, Arizona 85721, USA



(Received 4 March 2019; published 17 May 2019)

A general relativistic, stationary, and axisymmetric black hole in a four-dimensional asymptotically flat spacetime is fully determined by its mass, angular momentum, and electric charge. The expectation that astrophysically relevant black holes do not possess charge has resulted in a limited number of investigations of moving and charged black holes in the dynamical, strong-field gravitational (and electromagnetic) regime, in which numerical studies are necessary. Apart from having a theoretical interest, the advent of multimessenger astronomy with gravitational waves offers new ways to think about charged black holes. In this work, we initiate an exploration of charged binary black holes by generating valid initial data for general relativistic simulations of black hole systems that have generic electric charge and linear and angular momenta. We develop our initial data formalism within the framework of the conformal transverse-traceless (Bowen-York) technique using the puncture approach and apply the theory of isolated horizons to attribute physical parameters (mass, charge, and angular momentum) to each hole. We implemented our formalism in the case of a binary system by modifying the publicly available `TWOPUNCTURES` and `QUASILocalMEASURES` codes. We demonstrate that our code can recover existing solutions and that it has excellent self-convergence properties for a generic configuration of two black holes.

DOI: [10.1103/PhysRevD.99.104044](https://doi.org/10.1103/PhysRevD.99.104044)

I. INTRODUCTION

The successful detection of gravitational waves from the inspiral and merger of binary black holes by the LIGO-Virgo interferometers [1–5] was made possible not only by technological advancements in instrumentation but also by substantial improvements in theoretical modeling that furnished the gravitational-wave templates necessary for performing matched filtering [6–10]. To generate a bank of complete template signals, the equations of general relativity have to be solved during the late compact binary inspiral, merger, and postmerger phases because these events involve extreme gravitational fields, the description of which is not accurate with post-Newtonian methods. Obtaining an analytic solution to describe these systems during these dynamic stages is not possible. Therefore, numerical integration of the full Einstein equations provides the only viable avenue for understanding such relativistic astrophysical systems from first principles and for helping to build gravitational-wave templates during the most dynamical phases of their evolution.

Assuming that general relativity is the correct theory of gravity, the problem of two black holes is solved by integrating Einstein's equations in vacuum. Despite the simpler description of black hole spacetimes compared to spacetimes with matter, it took decades for the field of numerical relativity to mature enough to be able to stably evolve two black holes until merger [11–13]. Some of the issues that hindered the development were due to the highly nonlinear character of the Einstein equations, the coordinate freedom of general relativity, and the intrinsically singular nature of black holes. However, since the 2005 breakthrough, numerical relativity has advanced considerably with state-of-the-art codes that can simulate the inspiral and merger of uncharged binary black holes and extract gravitational waves with high precision (see, e.g., Refs. [14–20] and references therein). Numerical relativity furnishes invaluable information for gravitational-wave detection and analysis, which includes the development of templates (see, e.g., Refs. [9,10,21,22]) and the accurate parameter estimation of already detected events [23].

Apart from binary black holes, binary neutron stars and binary black hole–neutron stars are also the most promising gravitational-wave sources for currently operating interferometers [24]. In fact, among the 11 confirmed detections of gravitational waves so far [5], event GW170817 is

*gabrielebozzola@email.arizona.edu
†vpaschal@email.arizona.edu

attributed to the inspiral and merger of a binary neutron star [25] (although a binary black hole–neutron star cannot be ruled out [26–29] as a possibility). A complete simulation of compact binaries with matter requires the evolution of the spacetime coupled to matter, radiation/neutrinos, and electromagnetic fields in conjunction with detailed microphysics. A full solution including radiation/neutrinos without approximation is impossible at this time, and even with approximation, evolution of perfect fluids with existing numerical schemes involves density floors and other *ad hoc* prescriptions that are necessary to stabilize the calculations (see, e.g., Refs. [30,31]) but are designed such that their impact on the global solution is minimal. However, this means that, in a sense, simulations involving perfect fluids are not as “clean” as the ones in vacuum, which do not require *ad hoc* prescriptions. Nevertheless, many important results have been obtained through binary neutron star and binary black hole–neutron star simulations in full general relativity; see Refs. [32–38] for reviews (see also Ref. [39] for other applications of numerical relativity).

Interesting spacetimes that are as clean as vacuum spacetimes, but have received little attention in numerical relativity, are those described by Einstein-Maxwell’s theory. This theory involves only gravitational and electromagnetic fields, and the corresponding spacetimes are referred to as *electrovacuum*s or *electrovacs*. However, force-free electrodynamics has received some attention [40–47], but those simulations are not clean, in the sense that when the force-free conditions are violated during the evolution (typically in current sheets) one must interfere and enforce them to continue the calculations. On the other hand, electrovacuum spacetimes can be solved without physical approximations or *ad hoc* prescriptions, as the only assumption here is that electromagnetism and gravitation are described by the source-free Einstein-Maxwell equations. This simplification is the reason why these spacetimes have attracted numerous theoretical and analytic investigations for a long time, including the celebrated Kaluza-Klein theory [48,49] unifying gravity and electromagnetism.

Examples of interesting electrovacuum spacetimes are those with electrically charged black holes.¹ The case of a single charged nonrotating black hole is analytically solved by the Reissner-Nordström metric [50,51]. This solution has been extended to nonvanishing angular momentum in the Kerr-Newman spacetime [52], which generalizes the uncharged rotating black hole solution found by Kerr [53]. Another interesting class of solutions with multiple black holes is the static Majumdar-Papapetrou solution [54,55] that describes nonspinning black holes of which the electric

repulsion and gravitational attraction balance, producing a zero net force condition and thus equilibrium. The hypothesis of staticity was relaxed to simple stationarity by Refs. [56–58]. This list summarizes the known analytical solutions of the source-free Einstein-Maxwell equations in four-dimensional asymptotically flat spacetimes.

A reason why the source-free Einstein-Maxwell theory has been primarily confined to the realm of theoretical explorations is the fact that astrophysically relevant black holes are not believed to be electrically charged, as the charge would be neutralized by the surrounding plasma [59] or as result of a pair production through a Schwinger-like process [60]. Nonetheless, there are some viable mechanisms to have a black hole with nonzero charge. One example is the model proposed by Ref. [61], in which the charge is retained due to the presence of an external magnetic field. This is known as the “Wald mechanism.” It was shown in Ref. [61] that if an asymptotically uniform magnetic field B_0 can be sustained, a black hole with mass M spinning with angular momentum J would acquire an electric charge $Q = 2B_0J$ (measured in geometrized units²), which we can rewrite as $Q/M = 2B_0\chi M$ with $\chi = J/M^2$ the black hole dimensionless spin parameter. Since for black holes $\chi^2 \leq 1$, there exists a maximum possible charge-to-mass ratio in the Wald mechanism: $(Q/M) \leq (Q/M)_{\max} \equiv 2B_0M$ [61]. In the case of a solar mass black hole in the galactic magnetic field [62,63], the ratio has to be $Q/M \leq 10^{-24}$. The charge-to-mass ratio quantifies the deformation of the spacetime due to electromagnetism, so if it is very small, it means that the spacetime is well described by a vacuum (uncharged) black hole. Black holes with mass $M \gtrsim 10^9 M_\odot$ immersed in a magnetic field of order 10^{11} G would be needed to reach values of Q/M large enough to be relevant for the spacetime structure. Fields of such strength are expected to be found only in neutron stars. Based on the Wald mechanism, it has been recently proposed that a binary black hole–neutron star could provide a suitable environment to charge the black hole itself [64]. A second case in which charged black holes might occur in the Universe is immediately after the collapse of a compact star when the resulting hole might briefly retain some charge [65]. A similar scenario is the collapse of magnetized stars [66], which was also considered as candidate for fast-radio bursts [67]. Finally, charged black holes can emerge in more exotic theories associated with “hidden” gauge fields and elementary particles with a charge that is a fraction of the electron charge [68].

In spite of the apparently compelling reasons to believe that astrophysical black holes have practically zero net

¹It is also possible to include magnetic charges. This will not be done in the study presented in this paper, so we always take the term *charge* to mean *electric charge*. We note the extension of the work to include magnetic charges would be straightforward.

²The conversion factor between our units and the International System of Units (SI) is $c^2 G^{-\frac{1}{2}} (4\pi\epsilon_0)^{\frac{1}{2}} = 1.16 \times 10^{20} \text{ C km}^{-1}$, so $1M_\odot = 1.71 \times 10^{20} \text{ C}$, with c being the speed of light in vacuum, G being the gravitational constant, ϵ_0 being the vacuum permittivity, and M_\odot being the solar mass.

charge compared to their mass, it is still worth studying the source-free Einstein-Maxwell system to advance our comprehension of strong-field gravitation and electromagnetism in this largely unexplored territory. The interplay between electromagnetism and gravity in a highly dynamical spacetime, which can be probed only with numerical investigations, can offer a unique laboratory for both theoretical and more exotic astrophysical studies. For example, the inclusion of charge in highly relativistic collisions of black holes (see, for example, Refs. [69–72] for such studies with zero charge) would advance our understanding in a new direction never explored before. Another interesting application of dynamical electrovacuums is related to cosmic censorship. In a recent series of papers, it was argued that strong cosmic censorship can be violated by electrovacuums with a positive cosmological constant [73–75]. In contrast, the case without cosmological constant is not settled yet [76].

The coalescence and merger of charged black holes may present new interesting phenomenology. For instance, Ref. [77] proposed that the faint potential electromagnetic counterpart to GW150914 [78,79] might have been the result of the merger of charged black holes. Another hypothesized mechanism along similar lines invokes magnetic reconnection [80]. Subsequently, Ref. [81] tested the idea of Ref. [77] with relativistic simulations. However, the setup considered by the authors had some limitations: only equal-mass, equal-charge, nonrotating black holes were studied, and the initial data did not satisfy the constraints of the field equations. A more systematic study of this part of the parameter space of charged black holes requires that one starts with constraint-satisfying initial data for black hole configurations with arbitrary charge, mass ratio and linear and angular momenta.

The most common avenue for generating constraint-satisfying initial data is provided by the $3+1$ decomposition of spacetime [82,83]. In this approach, one casts the Einstein-Maxwell equations to an initial value problem in which the four-dimensional spacetime is foliated by successive time slices obtained via the dynamical evolution of the system.³ When performing this decomposition, both Maxwell’s and Einstein’s equations are split in two sets: the evolution and the constraint equations. The former move the system forward in time, whereas the latter must be satisfied at all times and must be used to generate the initial data for the evolution. In this paper, we primarily focus on the constraint equations.

Einstein-Maxwell’s theory was first cast in a $3+1$ decomposition by Ref. [85], and more than 25 years later, Ref. [86] proved that the evolution equations are symmetric hyperbolic and hence admit a well-posed initial value

problem. Moreover, the authors extended the work of Ref. [87] to generate initial data for electrically charged black holes at the moment of time symmetry (when the spacetime is invariant with respect to time reversal). Recent applications of this formalism are the head-on collisions by Refs. [88,89] (the interested reader can find several cogent additional reasons motivating the numerical study of charged black holes in these references). In these works, the authors evolved initial data generated with the same formalism described by Ref. [86] and were mostly interested in comparing the electromagnetic and gravitational emissions. Finally, the same group also investigated numerically the nonlinear stability of a Kerr-Newman black hole [90].

In this paper, we extend the work of Refs. [86,90] to generate initial data for charged, rotating, and moving black holes in a self-consistent way.⁴ We adopt the *conformal transverse-traceless* formalism [91] treating the black holes as punctures to solve for the metric and take advantage of the Reissner-Nordström solution in isotropic coordinates to solve for the electromagnetic fields. This strategy involves two major challenges. The first is that nonlinear partial differential equations have to be solved. This can be done only numerically for generic binary black hole configurations. To address this issue, we modify the `TWOPUNCTURE` code [92] to solve the resulting elliptic differential equations. The single-domain pseudospectral character of the code results in an accurate solution, and it is quickly convergent. The second challenge is that the physical interpretation of the results is not transparent. The parameters given as input for the algorithm (the *bare parameters*, such as mass and charge) in general are not actual *physical* quantities of the resulting black holes. Hence, we apply the theory of isolated horizons [93], which provides a quasilocal machinery for linking the bare black hole parameters with the physical ones and is suitable for simulations. We implement this numerically by modifying the `QUASILocalMEASURES` code [94].

We structure the paper as follows. In Sec. II, we review the mathematical tools necessary for generating initial data for charged black holes. In particular, we present the $3+1$ decomposition of Einstein-Maxwell’s theory and review the Reissner-Nordström solution in isotropic coordinates and the formalism of isolated horizons. In Sec. III, we solve the constraints with the conformal transverse-traceless technique. Our numerical implementation and tests are detailed in Sec. IV. Finally, Sec. V summarizes our findings and describes possible future research directions.

In Appendix A, we prepared a summary of the important equations and steps needed to generate initial data for generic systems of charged black holes. The Appendix

³It is worth mentioning that another common approach to building spacetimes in the computer is the *generalized harmonic formalism* [11,84].

⁴We note that the formalism outlined in this paper applies not only to electromagnetism but to any $U(1)$ charge (such as the one described in Ref. [68]).

provides a distilled overview of the analytic content of this paper. For the reader who is interested only in the gist of the algorithm/equations and the results of our work, we suggest they skip to Appendix A and then read Secs. IV A and IV B, in which we present our results.

A. Notation and conventions

We assume that gravity and electromagnetism are described by Einstein-Maxwell's theory [59], and we follow the same notation as in Ref. [95]. In particular, we use Einstein's summation convention, and the signature of the metric is $(-, +, +, +)$. We use geometrized units with $G = c = 1$, where c is the speed of light in vacuum and G is the gravitational constant. The unit of charge is defined so that the proportionality constant in Coulomb's law is 1 (for more details, see Ref. [96]). Indices a, b, c , and d run in the set $\{0, 1, 2, 3\}$, whereas the other latin letters, such as i, j or k , run in the set $\{1, 2, 3\}$ and refer to as spatial components. Parentheses and brackets in the indices mean symmetrization and antisymmetrization, respectively. We also use the abstract index notation [59]. We reserve the symbol ∇ for the four-dimensional covariant derivative associated with the spacetime metric g_{ab} and D for the three-dimensional covariant derivative, compatible with the spatial metric γ_{ij} . We denote the determinant of these metrics as $g = \det g_{ab}$ and $\gamma = \det \gamma_{ij}$. We prepend the symbol “(4)” to all the four-dimensional tensors, with the exception of the metric g_{ab} . For the completely antisymmetric Levi-Civita tensor, we use the convention that $\epsilon_{1230} = \sqrt{-g}$, and $\epsilon_{123} = \sqrt{\gamma}$, and denote the Levi-Civita symbol with $\bar{\epsilon}_{ijk}$ or $\bar{\epsilon}^{ijk}$.

II. FORMALISM

In this section, we describe the theoretical tools that we use later to generate initial data for arbitrary configurations of charged black holes. Specifically, in Sec. II A, we survey the $3+1$ decomposition of Einstein-Maxwell's equations, focusing on the constraint equations. Section II B reviews the Reissner-Nordström solution for a single charged stationary black hole in isotropic coordinates. Section II C summarizes the theory of isolated horizons, which we employ to assign the black hole physical properties: mass, charge, and angular momentum.

A. $3+1$ decomposition of Einstein-Maxwell

In this paper, we study systems described by the source-free Einstein-Maxwell equations [59]

$${}^{(4)}\mathcal{R}_{ab} - \frac{1}{2}g_{ab}{}^{(4)}\mathcal{R} = 8\pi{}^{(4)}T_{ab}^{\text{EM}}, \quad (1a)$$

$$\nabla_a{}^{(4)}F^{ab} = 0, \quad (1b)$$

$$\nabla_a{}^{(4)}\star F^{ab} = 0, \quad (1c)$$

where ${}^{(4)}\mathcal{R}_{ab}$ is the Ricci tensor associated with the metric g_{ab} , ${}^{(4)}\mathcal{R} = {}^{(4)}\mathcal{R}^a_a$, ${}^{(4)}F_{ab} = 2{}^{(4)}A_{[a,b]}$ is the Maxwell field-strength tensor, with ${}^{(4)}A_a$ the 4-potential, and ${}^{(4)}\star F_{ab}$ is its Hodge dual, defined by

$${}^{(4)}\star F^{ab} = \frac{1}{2}\epsilon^{abcd}{}^{(4)}F_{cd}. \quad (2)$$

The electromagnetic stress-energy tensor is

$$4\pi{}^{(4)}T_{ab}^{\text{EM}} = {}^{(4)}F_{ac}{}^{(4)}F_{bd}g^{cd} - \frac{1}{4}g_{ab}{}^{(4)}F_{cd}{}^{(4)}F^{cd}. \quad (3)$$

Solving the coupled Einstein-Maxwell equations in four dimensions is a challenging task. In particular, the form of Eqs. (1) is not suitable for a numerical solution. Therefore, we adopt the standard $3+1$ decomposition to express the equations as a Cauchy problem and cast them in a form amenable for numerical integration [97].

Assuming that the spacetime is described by a globally hyperbolic Lorentzian manifold \mathcal{M} with metric tensor g_{ab} , \mathcal{M} can be foliated by a family of spacelike nonintersecting hypersurfaces Σ_t , taken as level surfaces of a time function t . Let n^a be the future-directed, timelike unit vector normal to Σ_t . The projection operator along this vector is $n^a n_b$, whereas the one onto Σ_t is

$$\gamma_b^a = \delta_b^a + n^a n_b. \quad (4)$$

The induced metric on Σ_t is derived by applying twice the projection operator on g_{ab} , which yields

$$\gamma_{ab} = g_{ab} + n_a n_b. \quad (5)$$

The induced metric is purely spatial ($\gamma_{ab}n^b = 0$); it encodes the intrinsic curvature of the hypersurfaces Σ_t and can be used to define a spatial covariant derivative D_i on Σ_t .

Instead of working with the normal vector n^a , it is convenient to use the normalized time vector

$$t^a = \alpha n^a + \beta^a, \quad (6)$$

where α and β^a are the *lapse function* and *shift vector*. With these quantities, the spacetime metric assumes the Arnowitt-Deser-Misner (ADM) form [82,98]

$$ds^2 = -\alpha^2 dt^2 + \gamma_{ij}(dx^i + \beta^i dt)(dx^j + \beta^j dt). \quad (7)$$

The spatial metric is not sufficient to fully describe the curvature properties of the four-dimensional spacetime. The extrinsic curvature K_{ab} supplies the missing information by expressing how Σ_t is embedded in \mathcal{M} and is defined as

$$K_{ab} = -\gamma_a^c \gamma_b^d \nabla_c n_d. \quad (8)$$

Just like the induced metric (which we will also refer to as the 3-metric throughout), the extrinsic curvature is

purely spatial. The Riemann tensor can be expressed in terms of γ_{ij} and K_{ij} , and therefore Einstein's equations can be rewritten with only 3 + 1 quantities. The resulting 3 + 1 ADM (*à la* York) formalism [82,83] of general relativity consists of four constraints and 12 evolution equations. The constraints are the direct consequence of the integrability conditions that γ_{ij} and K_{ij} have to satisfy to have Σ_t properly embedded in \mathcal{M} . On the other hand, the evolution equations provide a prescription to move from one time slice to the next, provided a gauge choice is made. The evolution equations preserve the constraints; if the constraints are initially satisfied, they will always be satisfied. However, when they are not satisfied, the simulated system is not a solution of the Einstein equations. The same split into evolution equations and constraint equations holds for Maxwell's theory, too. In complete analogy to Einstein's theory, Maxwell's evolution equations preserve the Maxwell constraints, if the constraints are initially satisfied. For this reason, it is important to start with valid, constraint-satisfying initial data. In this work, we focus only on the constraint equations, precisely because our goal is the generation of valid initial data for general relativistic simulations in Einstein-Maxwell theory.

Let ${}^{(4)}T_{ab}^{\text{EM}}$ be the stress-energy tensor, and define

$$\mathcal{E} = n_a n_b {}^{(4)}T_{EM}^{ab}, \quad (9a)$$

$$S^i = -\gamma^{ij} n^a {}^{(4)}T_{aj}^{\text{EM}}. \quad (9b)$$

The Einstein constraints then become [97]

$$\mathcal{R} + K^2 - K_{ij}K^{ij} = 16\pi\mathcal{E}, \quad (10a)$$

$$D_j(K^{ij} - \gamma^{ij}K) = 8\pi S^i, \quad (10b)$$

with \mathcal{R} being the three-dimensional Ricci scalar associated with γ_{ij} and K being the trace of the extrinsic curvature. Equation (10a) is known as the *Hamiltonian* constraint, and Eq. (10b) is known as the *momentum* constraints.

Equations (10) are not the only constraints in Einstein-Maxwell's theory. As for Einstein's equations, a 3 + 1 split of Maxwell's equations must be performed.⁵ First, we introduce the electric and magnetic fields as seen by normal observers with 4-velocity n^a ,

$$E^a = {}^{(4)}F^{ab}n_b, \quad (11a)$$

$$B^a = {}^{(4)}\star F^{ab}n_b = \frac{1}{2}\epsilon^{abcd}n_b {}^{(4)}F_{cd}, \quad (11b)$$

which are both purely spatial ($n_a E^a = n_a B^a = 0$). The electromagnetic tensor becomes

$${}^{(4)}F_{ab} = n_a E_b - n_b E_a + \epsilon_{abcd}B^c n^d, \quad (12)$$

and its dual is

$${}^{(4)}\star F_{ab} = n_a B_b - n_b B_a - \epsilon_{abcd}E^c n^d. \quad (13)$$

With these decompositions, Maxwell's equations can be expressed in terms of 3 + 1 quantities. As in the case of the Einstein equations, the 3 + 1 split leads to evolution and constraint equations. In particular, the electromagnetic constraints are

$$D_a E^a = 0, \quad (14a)$$

$$D_a B^a = 0. \quad (14b)$$

The electromagnetic sector couples with the spacetime through the stress-energy tensor T_{EM}^{ab} , which is rewritten in terms of the 3 + 1 variables as

$$4\pi T_{EM}^{ab} = \frac{1}{2}(n^a n^b + \gamma^{ab})(E_c E^c + B_c B^c) + 2n^{(a}\epsilon^{b)cd}E_c B_d - (E^a E^b + B^a B^b), \quad (15)$$

where $\epsilon^{bcd} = n_a \epsilon^{abcd}$. Plugging Eq. (15) into the source terms of Eqs. (9), we find

$$4\pi\mathcal{E} = \frac{1}{2}(E_i E^i + B_i B^i), \quad (16a)$$

$$4\pi S^i = \epsilon^{ijk}E_j B_k, \quad (16b)$$

which are the familiar electromagnetic energy density and Poynting vector.

B. Reissner-Nordström spacetime

The Reissner-Nordström spacetime [50,51] describes an isolated nonrotating black hole with electric charge q and mass m [59]. This solution will be the base of our generalization to charged black hole systems. In Boyer-Lindquist coordinates (t, r, θ, ϕ) , the Reissner-Nordström metric is given by

$$ds^2 = -\left(1 - \frac{2m}{r} + \frac{q^2}{r^2}\right)dt^2 + \left(1 - \frac{2m}{r} + \frac{q^2}{r^2}\right)^{-1}dr^2 + r^2(d\theta^2 + \sin^2\theta d\phi^2), \quad (17)$$

and the electromagnetic potential of the solution is

$${}^{(4)}A = -\frac{q}{r}dt. \quad (18)$$

In the following sections, we will adopt the puncture approach, so we transform the Boyer-Lindquist coordinates to isotropic ones. To do so, we define a new radial coordinate R , satisfying

⁵A more detailed derivation of the three-dimensional Maxwell equations from the four-dimensional ones can be found in the Appendix of Ref. [86] (see also Ref. [99]).

$$r = R \left(1 + \frac{m}{R} + \frac{R_H^2}{R^2} \right), \quad (19)$$

with $R_H = \frac{1}{2} \sqrt{m^2 - q^2}$ the radius of the black hole horizon in isotropic coordinates. The metric then assumes the form

$$ds^2 = -\Psi^{-4} dt^2 + \Psi^4 \delta_{lk} dx^l dx^k, \quad (20)$$

with δ_{lk} being the flat Euclidean metric and Ψ being the conformal factor defined as

$$\Psi = \sqrt{1 + \frac{m}{R} + \frac{R_H^2}{R^2}} = \sqrt{\left(1 + \frac{m}{2R}\right)^2 - \left(\frac{q}{2R}\right)^2}. \quad (21)$$

As is clear from Eq. (20), the spatial metric is manifestly conformally flat in isotropic coordinates. Moreover, there is no magnetic field, and the electric field has only an R component,

$$E^R = \Psi^{-6} \frac{q}{R^2}. \quad (22)$$

As a result, the Poynting vector defined in Eq. (16b) is identically zero everywhere.

C. Isolated horizons

Once the constraint equations are solved, it is important to interpret the physical configuration to which the initial data correspond. This can be achieved by locating the black hole apparent horizons and applying the theory of *isolated horizons* [93] (see Ref. [100] for a review). Isolated horizons provide a quasilocal notion of the black hole physical properties. In this section, we review basic identities of the formalism, including, in particular, the electric charge of the horizon, and the electromagnetic-field contribution to angular momentum, elements that have not received much attention in numerical relativity applications [94,101].

Isolated horizons have several desirable features. For instance, they always lie inside the event horizon, to which they reduce for stationary spacetimes, and they imply the existence of a future singularity [102,103]. Most relevant for our purpose, they provide well-defined notions of mass, charge, and angular momentum. For spacetimes with suitable symmetries, these quasilocal physical quantities coincide with the global ones defined from conservation laws (for example, via ADM integrals), as we verify this explicitly for the Reissner-Nordström case in Appendix B. However, in general, the quasilocal definitions and those at infinity differ [93]. Furthermore, the formalism does not provide a quasilocal definition of linear momentum due to the lack of a meaningful notion of space-translational symmetry in curved spacetime [100,104].

Here, we follow closely Ref. [94] in using isolated horizons to assign black hole physical parameters. Given a spatial section \mathcal{S} of an isolated horizon, the variables we are interested in are defined as follows. First, the areal radius is given by

$$R_S = \left(\frac{1}{4\pi} \int_{\mathcal{S}} \epsilon \right)^{\frac{1}{2}}, \quad (23)$$

where ϵ is the area 2-form on the 2-surface, given by $\epsilon = \frac{1}{2} \sqrt{\mathfrak{q}} \bar{\epsilon}_{ab} dx^a \wedge dx^b$, where \mathfrak{q}_{ab} is the induced metric on the horizon, $\mathfrak{q} = \det \mathfrak{q}_{ab}$, and $\bar{\epsilon}_{ab}$ is the two-dimensional antisymmetric symbol. $\int_{\mathcal{S}} \epsilon$ is the surface area of the horizon.

Next, the definition of the angular momentum is based on an approximate rotational killing vector field φ^a on the 2-surface [93],

$$J_S = -\frac{1}{8\pi} \int_{\mathcal{S}} (\varphi \cdot \omega) \epsilon + 2(\varphi \cdot {}^{(4)}A) {}^{(4)}\star F, \quad (24)$$

where ω is the form that satisfies the condition $t^a \nabla_a k^b = t^a \omega_a k^b$ for any vector t^a tangent to \mathcal{S} , with k^b being the outgoing future-directed vector normal to \mathcal{S} . By construction of k^b , ω always exists [93]. The two terms in the right-hand side of Eq. (24) are the gravitational and electromagnetic contribution to the horizon angular momentum.

The charge is defined by means of Gauss's law,

$$Q_S = \frac{1}{4\pi} \int_{\mathcal{S}} {}^{(4)}\star F, \quad (25)$$

and finally, the gravitational mass of the isolated horizon is given by

$$M_S = \frac{1}{2R_S} [(R_S^2 + Q_S^2)^2 + 4J_S^2]^{\frac{1}{2}}. \quad (26)$$

For Kerr-Newman black holes, this formula perfectly reduces to the equation that relates total mass, irreducible mass, charge, and angular momentum [105].

The definitions of angular momentum and charge involve four-dimensional quantities, but during simulations with the 3 + 1 formalism, it is more convenient to use 3 + 1 variables. In Ref. [94], it was shown that the gravitational contribution to the horizon angular momentum can be computed using an ADM-like formula,

$$J_S^{\text{GR}} = -\frac{1}{8\pi} \int_{\mathcal{S}} (\varphi \cdot \omega) \epsilon = \frac{1}{8\pi} \int_{\mathcal{S}} \varphi^a R^b K_{ab} \epsilon, \quad (27)$$

where R^a is the spatial unit vector normal to \mathcal{S} . The electromagnetic component of the angular momentum $J_S^{\text{EM}} = J_S - J_S^{\text{GR}}$ depends on both ${}^{(4)}A$ and ${}^{(4)}\star F$. The first is directly accessible if instead of the electric and magnetic

fields one evolves the vector potential [106–110], whereas the second has components

$${}^{(4)}\star F_{ab} = (2n_{[a}B_{b]} - \epsilon_{abc}E^c). \quad (28)$$

When integrated over a spatial 2-surface, the term $2n_{[a}B_{b]}$ does not contribute because $n_a = (-\alpha, 0, 0, 0)$. Therefore, the electromagnetic contribution to the horizon angular momentum becomes

$$J_S^{\text{EM}} = -\frac{1}{4\pi} \int_S (\varphi \cdot {}^{(4)}A) \frac{1}{2!} \epsilon_{abc} E^c dx^a \wedge dx^b, \quad (29)$$

where $\epsilon_{abc} = n^d \epsilon_{abcd}$. By use of Eqs. (28) and (25) for the charge becomes

$$Q_S = \frac{1}{4\pi} \int_S \frac{1}{2!} \epsilon_{abc} E^c dx^a \wedge dx^b. \quad (30)$$

These definitions provide a complete characterization of black holes during a general relativistic simulation with the $3+1$ decomposition. An example of how the integrations above are performed is in Appendix C.

III. SOLVING THE CONSTRAINT EQUATIONS

To solve the constraint equations, we adopt the conformal transverse-traceless approach, also referred to as the Bowen-York technique [91]. The goal of this method is to expose and specify degrees of freedom containing physical information about the system by applying conformal transformations on the spatial quantities and working directly on the *conformal* variables instead of the physical ones.

The first step in the method is to conformally decompose γ_{ij} by introducing the conformal factor ψ and metric $\bar{\gamma}_{ij}$,

$$\gamma_{ij} = \psi^4 \bar{\gamma}_{ij}. \quad (31)$$

In the following, we use an overbar to indicate conformal quantities.

A common assumption when generating multiple black hole initial data is that the spatial metric is conformally flat [86,97,111,112]. In other words, we fix the conformal three-dimensional metric $\bar{\gamma}_{ij}$ to be the flat Euclidean metric δ_{ij} (in Cartesian coordinates). This choice greatly simplifies computations, and it is a good approximation for the systems we are interested in studying, in spite of the fact that conformally flat spatial slices of the Kerr metric do not exist [113]. Conformal flatness limits the maximum equilibrium value that the black hole dimensionless spin can attain [15,112], but values of order 0.9 are completely achievable. Thus, we do not anticipate this approximation to impose severe constraints on the equilibrium values of the black hole spin and charge. Considering what happens in the uncharged case [114,115], we expect that conformal

flatness will generate initial data with spurious gravitational radiation in the charged black hole cases, too. Nonetheless, this is not a major concern since in dynamical simulations the system is evolved until this “junk” radiation propagates away, and the fields relax to their quasiequilibrium values.

In addition to the conformal decomposition of the metric, it is also useful to transform the extrinsic curvature K_{ij} by separating it into its traceless A_{ij} and trace ($K = K^i_i$) parts,

$$K_{ij} = A_{ij} + \frac{1}{3} \gamma_{ij} K. \quad (32)$$

Following standard practice, we adopt the maximal slicing condition $K = 0$ [116] and introduce a conformal, traceless extrinsic curvature \bar{A}_{ij} as

$$K_{ij} = A_{ij} = \psi^{-2} \bar{A}_{ij}. \quad (33)$$

Then, \bar{A}_{ij} can be split into a transverse-traceless part and a longitudinal part,

$$\bar{A}^{ij} = \bar{A}_{\text{TT}}^{ij} + \bar{A}_{\text{L}}^{ij}. \quad (34)$$

We set $\bar{A}_{\text{TT}}^{ij} = 0$, which corresponds to suppressing the radiative degrees of freedom, so

$$\bar{A}^{ij} = \bar{A}_{\text{L}}^{ij}. \quad (35)$$

The longitudinal part can always be expressed in terms of a vector V as

$$\bar{A}^{ij} = \bar{A}_{\text{L}}^{ij} = 2\delta^{ik}\delta^{jh}V_{(h,k)} - \frac{2}{3}\delta^{ij}\partial_k V^k, \quad (36)$$

where Cartesian coordinates are adopted. Going back to Eq. (33), the extrinsic curvature is given by

$$K_{ij} = \psi^{-2} \left(2V_{(i,j)} - \frac{2}{3}\delta_{ij}\partial_k V^k \right). \quad (37)$$

We already exploited much of the freedom we had in specifying variables during the previous steps. Under these assumptions, we just need the vector V^i and the conformal factor ψ to fully determine γ_{ij} and K_{ij} , and the constraint Eqs. (10) take the form

$$\nabla^2 \psi + \frac{1}{8} \psi^{-7} \bar{A}_{ij} \bar{A}^{ij} + 2\pi \psi^5 \mathcal{E} = 0, \quad (38a)$$

$$(\nabla^2 V)^i + \frac{1}{3} \delta^{ij} \partial_j (\partial_k V^k) - 8\pi \psi^{10} S^i = 0, \quad (38b)$$

where $\nabla^2 = \partial_k \partial^k$.

Next, we turn to the electromagnetic sector of the problem. We rescale the electromagnetic fields as in Ref. [86]

$$\begin{aligned}\bar{E}^i &= \psi^6 E^i, & \bar{E}_i &= \psi^2 E_i, \\ \bar{B}^i &= \psi^6 B^i, & \bar{B}_i &= \psi^2 B_i.\end{aligned}\quad (39)$$

The factor ψ^6 is chosen in order to have $D_i E^i = \psi^{-6} \partial_i \bar{E}^i$, where we used the fact that for any vector v^i it holds true that $D_i v^i = \gamma^{-1/2} \partial_i (\sqrt{\gamma} v^i)$. The Maxwell constraints (14) read

$$\partial_i \bar{E}^i = 0, \quad (40a)$$

$$\partial_i \bar{B}^i = 0. \quad (40b)$$

These equations do not depend on the conformal factor ψ , so the electromagnetic constraints can be solved independently from the spacetime ones. Moreover, the equations are linear; hence, we can superpose solutions.

Having fixed the conformal scalings of the E^i and B^i fields, the source terms \mathcal{E} and S^i of the Einstein constraints conformally transform as

$$\mathcal{E} = \psi^{-8} \bar{\mathcal{E}}, \quad (41a)$$

$$S^i = \psi^{-10} \bar{S}^i, \quad (41b)$$

where

$$4\pi \bar{\mathcal{E}} = \frac{1}{2} (\bar{E}_i \bar{E}^i + \bar{B}_i \bar{B}^i), \quad (42a)$$

$$4\pi \bar{S}^i = \bar{\epsilon}^{ijk} \bar{E}_j \bar{B}_k. \quad (42b)$$

With these redefinitions, the Einstein constraints become

$$\nabla^2 \psi + \frac{1}{8} \psi^{-7} \bar{A}_{ij} \bar{A}^{ij} + 2\pi \psi^{-3} \bar{\mathcal{E}} = 0, \quad (43a)$$

$$(\nabla^2 V)^i + \frac{1}{3} \delta^{ij} \partial_j (\partial_k V^k) - 8\pi \bar{S}^i = 0. \quad (43b)$$

The problem is now greatly simplified because the momentum constraints do not depend on ψ , are linear in V^i , and along with the Hamiltonian constraint have decoupled from the Maxwell constraints.

Next, we exploit the linearity of Eq. (43b) by decomposing V^i as

$$V^i = V_{0,\text{GR}}^i + V_{\text{EM}}^i, \quad (44)$$

where $V_{0,\text{GR}}^i$ solves the homogeneous Eq. (10b) (when $\bar{S}^i = 0$) and V_{EM}^i solves the inhomogeneous one.⁶ The first term does not contain any reference to the

electromagnetic sector of the problem. Thus, as in Ref. [92], we choose

$$V_{0,\text{GR}}^i = \sum_{n=1}^{N_p} \left(-\frac{7}{4} \frac{P_n^i}{R_n} - \frac{1}{4} \delta_{jk} x_n^j P_n^k \frac{x_n^i}{R_n^3} + \frac{\bar{\epsilon}^i{}_{jk} x_n^j S_n^k}{R_n^3} \right), \quad (45)$$

with $R_n = |\mathbf{x} - \mathbf{x}_n|$ being the Euclidean coordinate distance from puncture n , where \mathbf{x}_n is the location of the n th puncture, and P_n^i and S_n^k are its linear and angular momenta, respectively. Equation (45) solves the homogeneous version of Eq. (43b), and it is known that for suitable single black hole solutions $P_{\text{ADM}}^i = P^i$ and $J_{\text{ADM}}^i = S^i$, with P_{ADM} and J_{ADM} being the ADM linear and angular momenta evaluated at infinity [91,92], respectively. By use of the decomposition (44), the momentum constraints further reduce to three decoupled linear equations for V_{EM}^i , effectively replacing Eq. (43b) with

$$\nabla^2 V_{\text{EM}}^i + \frac{1}{3} \delta^{ij} \partial_j (\partial_k V_{\text{EM}}^k) - 8\pi \bar{S}^i = 0. \quad (46)$$

We also manipulate the Hamiltonian constraint (43a) further by separating the singular part of the conformal factor from the finite one u , motivating our ansatz based on the conformal factor of the Reissner-Nordström spacetime in Eq. (21),

$$\psi = \left[\left(1 + u + \sum_{n=1}^{N_p} \frac{M_n}{2R_n} \right)^2 - \left(\sum_{n=1}^{N_p} \frac{Q_n}{2R_n} \right)^2 \right]^{\frac{1}{2}}. \quad (47)$$

We introduce the following abbreviations for compactness:

$$\eta = \sum_{n=1}^{N_p} \frac{M_n}{2R_n}, \quad \varphi = \sum_{n=1}^{N_p} \frac{Q_n}{2R_n}, \quad \kappa = 1 + u + \eta. \quad (48)$$

Therefore, the conformal factor becomes

$$\psi = \sqrt{\kappa^2 - \varphi^2}. \quad (49)$$

Equation (47) is essentially an ansatz that states that our solution is a superposition of Reissner-Nordström black holes plus corrections (in u), which parallels what is performed in the uncharged case [117].

Expanding Eq. (43a), we reach

$$\begin{aligned}\kappa \nabla^2 u + \partial_a \kappa \partial^a \kappa - \partial_a \varphi \partial^a \varphi - \partial_a \psi \partial^a \psi + \frac{1}{8} \psi^{-6} \bar{A}_{ij} \bar{A}^{ij} \\ + 2\pi \psi^{-2} \bar{\mathcal{E}} = 0.\end{aligned}\quad (50)$$

In deriving the last expression, we used the fact that the Laplacian of η and φ is zero. Equation (50) is a second-order, nonlinear elliptic partial differential equation in u that depends on V_{EM}^i through the term $\bar{A}_{ij} \bar{A}^{ij}$. Now, the

⁶The subscript 0 does not indicate any component, but it reminds us that the field is a solution of the homogeneous equation.

momentum and Hamiltonian constraints (10) have been reexpressed as elliptic equations (46) and (50) for V_{EM}^i and u . The associated boundary conditions are found from the assumption of asymptotic flatness so that u and V_{EM}^i have to go to zero at spatial infinity. In this paper, we assume that u and V_{EM}^i are regular everywhere, and thus they can be found with our numerical scheme.

The problem of generating valid initial data for multiple charged black holes is now reduced to solving Eqs. (46) and (50), which is done once Maxwell-compliant electromagnetic fields are found. In this paper, we assume that each puncture is endowed with a Reissner-Nordström electromagnetic field, and hence the total conformal electric field is a superposition of Reissner-Nordström electromagnetic fields in isotropic coordinates, i.e.,

$$\bar{E}^i = \sum_{n=1}^{N_p} \frac{Q_n}{R_n^2} \hat{R}_n^i, \quad (51)$$

where \hat{R}_n is the radial unit vector centered on the n th puncture. In the case of a single, nonrotating black hole with zero linear momentum, our choice of Reissner-Nordström fields exactly produces a spatial slice of that solution, since the constraints are solved by $V_{\text{GR}} = V_{\text{EM}} = 0$, and $u = 0$ [so $\psi = \Psi$, where Ψ is given in Eq. (21)]. For systems of spinning black holes with linear momenta, the superposition of Reissner-Nordström fields is a first approximation to the equilibrium electromagnetic field generated by these configurations. As for the gravitational fields generated in the puncture approach (and the gauge fields), we expect that the time evolution will relax our electromagnetic-field initial data to their quasiequilibrium values on a light-crossing timescale. An advantage of choosing Reissner-Nordström electromagnetic fields is that they allow for a clear description of each black hole in the system with a specific charge as the isolated horizon value Q_S equals the “bare” charge entering Eq. (51). In addition, since there is no magnetic field, the source term of Eq. (46) vanishes, and so $V_{\text{EM}} = 0$ (even for multiple black holes with linear and angular momenta). Thereby, this choice ensures that there are no electromagnetic contributions to the extrinsic curvature, implying that the parameters entering Eq. (45) can be still interpreted as $P_{\text{ADM}}^i = P^i$ and $J_{\text{ADM}}^i = S^i$.

The choice of Reissner-Nordström electromagnetic fields is by no means unique. Another possibility is Kerr-Newman fields in quasi-isotropic coordinates. We present a detailed discussion of this case and the complexities associated with it in Appendix D.

IV. NUMERICAL IMPLEMENTATION

We implement the formalism outlined in the previous sections by modifying the `TWO PUNCTURES` [92] and `QUASILocalMEASURES` open-source codes [94]. The

software is run within the `CACTUS` infrastructure [118], and all physical variables are interpolated on a `CARPET` grid [119,120]. Black hole apparent horizons are found with `AHFINDERDIRECT` [121].

The main component in our software stack is `TWOCHARGEDPUNCTURES`, which is used to generate initial data for two punctures located at $(\pm b, 0, 0)$, given the bare black hole properties (M_n, Q_n, P_n^i, S_n^i) . This code implements a pseudospectral collocation method that solves the constraint equations (46) and (50) to find u and V_{EM}^i .

In what follows, we adopt Reissner-Nordström electromagnetic fields. Since there is only an electric field, $\bar{S}^i = 0$ in Eq. (46), and the momentum constraint is trivially satisfied by $V_{\text{EM}}^i = 0$. Hence, we only need to solve the Hamiltonian constraint (50).

`TWOCHARGEDPUNCTURES` implements a single domain pseudospectral method that covers all \mathbb{R}^3 with spatial infinity on the grid. This region is parametrized by the coordinates (A, B, ϕ) , with $A, B \in [-1, 1]$ and $\phi \in [0, 2\pi]$. To be more specific, the code uses a system of bispherical coordinates that transform to the usual Cartesian ones with the law⁷

$$x = b \frac{(1+A)^2 + 4}{(1+A)^2 - 4} \frac{2B}{1+B^2}, \quad (52a)$$

$$y = b \frac{4(1+A)}{4 - (1+A)^2} \frac{1-B^2}{1+B^2} \cos \phi, \quad (52b)$$

$$z = b \frac{4(1+A)}{4 - (1+A)^2} \frac{1-B^2}{1+B^2} \sin \phi, \quad (52c)$$

where the x axis is along the line connecting the two punctures. Equations (52) describe a set of cylindrical-like coordinates around the x axis with a radius that depends on both A and B .

The coordinates (A, B, ϕ) live on a compact grid where spatial infinity corresponds to $A = 1$, which makes it straightforward to impose the desired outer boundary conditions ($u \rightarrow 0$ at infinity). This condition is enforced by solving the equations for an auxiliary variable \mathcal{U} defined as $u = (A-1)\mathcal{U}$. The code expands \mathcal{U} in Chebyshev polynomials along A and B and adopts a Fourier basis along ϕ . The coordinates are discretized with n_A , n_B , and n_ϕ grid points chosen as the zeros of Chebyshev polynomials $T_{n_A}(x)$, $T_{n_B}(x)$ and of the sine function $\sin(n_\phi \phi)$. The coefficients of the spectral expansion are found by evaluating the relevant equation on the

⁷This parametrization is slightly different than what is done in Ref. [92]. The spectral expansion used here treats A and B on equal footing, i.e., the spectral decomposition in A and B uses the same Chebyshev polynomial basis, unlike what is reported in Ref. [92].

collocations points and solving the corresponding multi-dimensional nonlinear system with a modified Newton-Raphson method [122] (more details on how this is done can be found in Sec. II of the original paper [92]). We consider the equations to be solved, when the residuals are smaller than a threshold value. To choose this threshold value, we solve for increasingly smaller values of this threshold and compute the ADM and the horizon masses. When these masses have converged to within one part in 10^6 , we consider the solution converged.

With the equations solved and u known, TWOCHARGEDPUNCTURES reverts back to the physical fields using Eqs. (37), (39) (44), (45), and (47). We then spectrally interpolate the physical fields on a CARPET grid where AHFINDERDIRECT is subsequently run to locate the apparent horizons. Once the horizons are found, we compute the mass, charge, and angular momentum of each black hole with our version of QUASILocalMEASURES, which we call QUASILocalMEASURESEM and which implements the formalism of isolated horizons for the full Einstein-Maxwell theory as reviewed in Sec. II C. Moreover, having the spectral expansion of the fields, we can interpolate them at a very large radius to compute the ADM mass and the linear and angular momenta.

A. Code validation

We validate our approach and numerical implementation with a series of tests that is presented in the section.

We report our results in terms of the input bare mass M of the punctures, which is the only mass known *a priori*. In all the runs, we confine the black hole in a region where the CARPET grid resolution is $\Delta x_i = 0.0078M$, which usually guarantees that the diameter of the horizon is resolved by about 100 points, making it easily found by AHFINDERDIRECT. We also fix the resolution of the AHFINDERDIRECT grid to be 79 points in the azimuthal direction and 39 in the meridional direction. We have confirmed that the resolution on the AHFINDERDIRECT grid has a negligible impact in our results. In the cases presented here, doubling the AHFINDERDIRECT grid resolution introduces a variation in the computed parameters of order 0.01%. We compute ADM integrals by spectrally interpolating our fields on a sphere of radius $10000M$, discretized with 256 points in both the meridional and azimuthal directions.

As a first test, we made sure that our modified code with zero charge, TWOCHARGEDPUNCTURES, produces the same output as the standard open-source TWOPUNCTURES code. This is not a trivial test because the equations used in our code and in the original one are different, having different numerical properties, even though they are mathematically equivalent. In particular, our formulation is more susceptible to numerical instabilities due to the finite-arithmetic error in regions close to the puncture. The reason for this is that our equations have terms that are not present in the

original code but that should perfectly cancel out when $Q = 0$. Such a numerical cancellation near the punctures is not trivial. However, the result of the test with different spectral resolutions shows that the two implementations agree at the round-off-error level for punctures with no charge.

Another key test that our code successfully passes consists in recovering the only conformally flat analytical solutions known: the Reissner-Nordström and the case of two black holes with the same charge-to-mass ratio (see Appendix E for more details), both of which are found with $u = 0$. We find the solution $u = 0$ is recovered to machine precision everywhere outside the horizons, and it is non-identically zero only very close to the punctures, again due to numerical precision.

The next test for TWOCHARGEDPUNCTURES is reproducing the numerical solution found by Ref. [86] for two nonrotating black holes with opposite charge-to-mass ratio starting at rest. Figure 1 reports the value of u along the x , y , and z axes for a system of two punctures with the same mass but opposite charge ($Q_1 = -Q_2 = 0.5M$). We graphically superposed our plot with Fig. 1 in Ref. [86], finding perfect agreement.

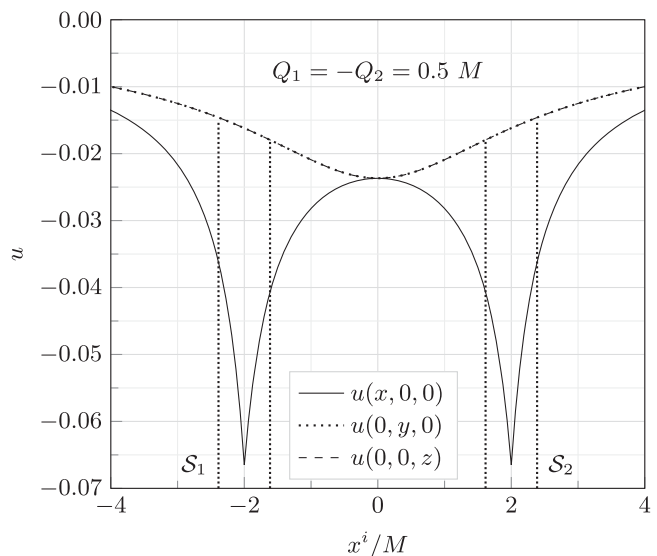


FIG. 1. u along the different coordinate axes (solid line for the x axis and dotted and dashed lines for the y and z axes, respectively) for two punctures with equal mass and opposite charge $Q_1 = -Q_2 = 0.5M$ located on the x axis at $\pm 2M$. This configuration is generated with a spectral grid resolution $n_A = n_B = n_\varphi = 64$. We graphically compared our solution to the solution in Ref. [86] and found that the curves shown here perfectly match the solution of Ref. [86]. The horizons have areal radius $R_{S_1} = R_{S_2} = 0.387M$ as defined by Eq. (23). The vertical dotted lines represent the coordinate radius of the horizons as found by AHFINDERDIRECT. We note that the black hole horizons in binary black holes are generally nonspherical; see, e.g., Ref. [123].

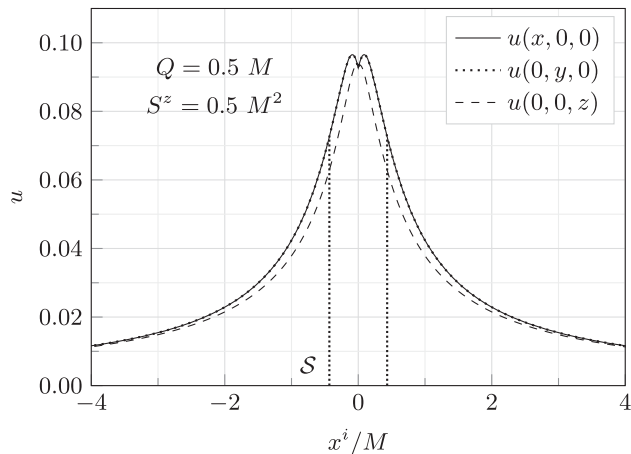


FIG. 2. u along the coordinate axes for a single puncture with charge $Q = 0.5M$ rotating around the z axis with angular momentum $S^z = 0.5M^2$. The plot corresponds to spectral grid resolution $n_A = n_B = n_\phi = 64$. The horizon has areal radius $R_S = 0.433M$. The different styles of curves have the same meanings as in Fig. 1.

Continuing the progression of complexity in the considered systems, we generate a single puncture with angular momentum but no linear momentum and one with linear momentum but no angular momentum (Figs. 2 and 3, respectively). In these single-black hole cases, we compare the horizon mass with the ADM mass measured at infinity, and we find agreement of order 0.1% even with resolution as low as $n = 16$. The same is true for the ADM angular momentum and the horizon spin, as computed with QUASILocalMEASURESEM. We repeated these two tests by aligning the linear and angular momentum vectors once

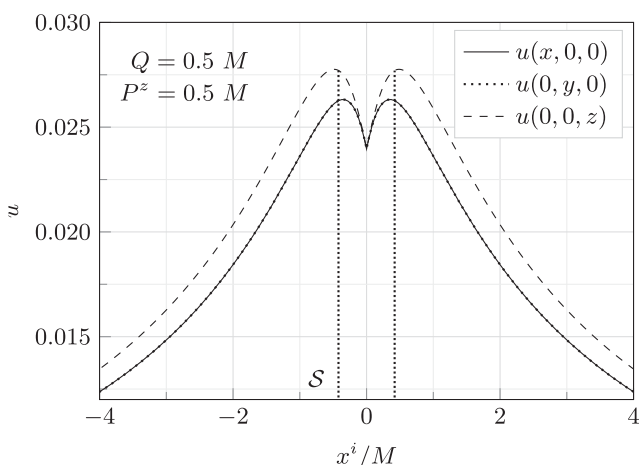


FIG. 3. u along the coordinate axes for a single puncture with charge $Q = 0.5M$ with linear momentum $P^z = 0.5M$. The plot corresponds to spectral grid resolution $n_A = n_B = n_\phi = 64$. The horizon has areal radius $R_S = 0.421M$. The different styles of curves have the same meanings as in Fig. 1.

along the x direction and once along the z direction to ensure that the built-in asymmetry in the coordinates [Eqs. (52)] does not spoil expected symmetries in symmetric configurations. By doing this, we find that the solutions are rotationally invariant to better than one part in 10^6 for a resolution $n = 32$ or higher.

B. Convergence

Finally, we considered the generic system shown in Fig. 4. This is formed by two equal-mass black holes with charge $Q_1 = -0.3M$ and $Q_2 = 0.5M$. Both black holes are spinning with angular momentum $S_1^z = S_2^z = 0.5M^2$. The black holes also have linear momentum $P_1^x = P_2^z = -0.5M$. The solution for u for this system is depicted in Fig. 5. With QUASILocalMEASURESEM, we find that the quasilocal angular momenta (charges) agree with their bare counterparts to within one part in 10^4 (10^8). We find that the mass of the first horizon is $1.187M$ and the second is $1.202M$. The total (ADM) mass of the system is $2.337M$, and the difference between this value and the sum of the individual masses is the binding energy.

This system is used to study the self-convergence properties of the code. In particular, we consider the maximum relative error of u with respect to a reference

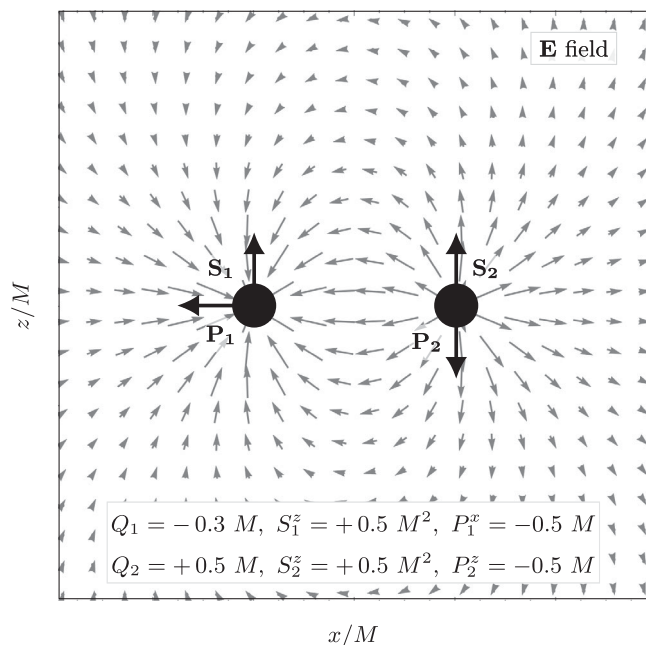


FIG. 4. Electric-field lines on the $x - z$ plane for two charged punctures. The first (left) black hole has charge $Q_1 = -0.3M$, linear momentum $P_1^x = -0.5M$, and spin angular momentum $S_1^z = 0.5M^2$. The second (right) black hole has $Q_2 = 0.5M$, linear momentum $P_2^z = -0.5M$ and spin angular momentum $S_2^z = 0.5M^2$. The black disks depict the apparent horizon of each black hole, which set the scale in the plot. This is the test case used in the self-convergence test reported in Fig. 6.

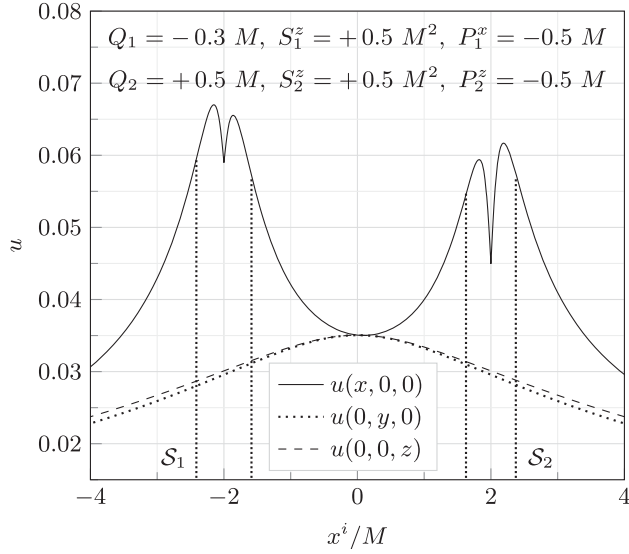


FIG. 5. u along the coordinate axes for two punctures with charge $Q_1 = -0.3M$ and $Q_2 = 0.5M$. The first black hole has linear momentum $P_1^x = -0.5M$ and spin angular momentum $S_1^z = 0.5M^2$. The second black hole has linear momentum $P_2^z = -0.5M$ and spin angular momentum $S_2^z = 0.5M^2$. The electric-field lines are reported in Fig. 4. The plot corresponds to spectral grid resolution $n_A = n_B = n_\phi = 64$. This system is used for the self-convergence test in Fig. 6. The horizons have radii $R_{S_1} = 0.412M$ and $R_{S_2} = 0.373$ and quasilocal masses $M_{S_1} = 1.187M$ and $M_{S_2} = 1.202M$. The different styles of curves have the same meanings as in Fig. 1.

solution at high resolution N . For this, we sampled u on a set of points \mathcal{T} and computed the infinity norm

$$\|\Delta_n^N u\|_\infty^{\mathcal{T}} = \max_{\mathbf{x} \in \mathcal{T}} \left| \frac{u^n(\mathbf{x}) - u^N(\mathbf{x})}{u^N(\mathbf{x})} \right|. \quad (53)$$

We choose \mathcal{T} as the set of points in which spheres of radii $1M$, $2M$, $5M$, $10M$, $100M$, and $1000M$ intersect the coordinate axes for $x > 0$, $y > 0$, $z > 0$.

We set as a reference solution (N) one obtained at high-resolution with $n_A = n_B = n_\phi = n = 64$, which is between $n = 50$ and $n = 70$ that were used for self-convergence tests in the original TWO-PUNCTURES code [92]. Here, we simply choose resolutions which are multiples of 4, but our results do not depend on this choice. Our convergence test (Fig. 6) shows that the algorithm is robust; u quickly converges to its high-resolution value. The code converges approximately at sixth order. We also verified that the code exhibits the same convergence properties when we repeat the convergence test with $Q_1 = Q_2 = 0$, which also agree with the convergence properties of the original TWO-PUNCTURES code [92]. The convergence of u also results in excellent convergent behavior for both the ADM mass and momenta and the horizon properties as computed by QUASILocalMEASURESEM.

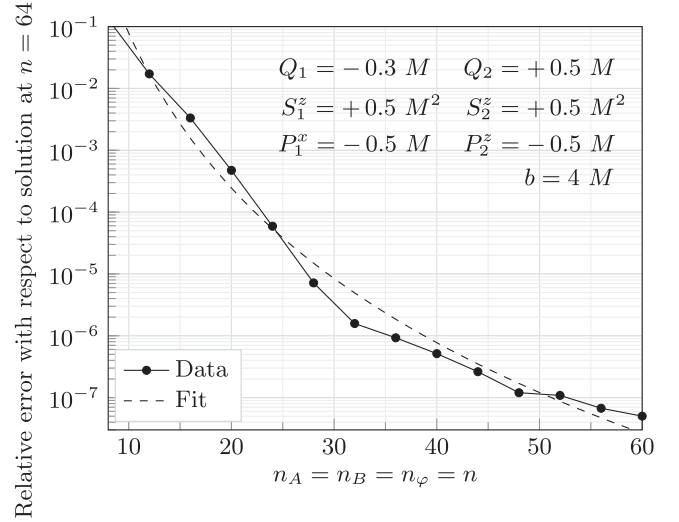


FIG. 6. Convergence properties of the algorithm measured by computing the maximum relative error on u $\|\Delta_n^{64} u\|_\infty^{\mathcal{T}}$ over the test set \mathcal{T} (formed by points at distances $1M$, $2M$, $5M$, $10M$, $100M$, and $1000M$ on the different coordinate axes). See Fig. 4 for the geometric setup and black hole parameters used for this test. The dashed line shows that the code is approximately sixth-order convergent. All the other physical properties (such as the ADM mass and momenta and the horizon quantities) inherit this excellent convergence behavior from u .

V. CONCLUSIONS

Gravitational waves offer new opportunities to study the Universe that are not accessible with electromagnetic or neutrino astronomy. In this landscape, numerical-relativity simulations are a powerful tool to gain insight into the properties and the characteristics of both the waves and their sources. The majority of numerical-relativity simulations of black holes to date do not treat the electric charge. This is because it is believed that astrophysically relevant black holes should have a charge that is negligibly small compared to the mass. For this reason, there are no studies of highly dynamical electrovacuum spacetimes that involve the inspiral and merger of binary black holes with charge and spin. Nevertheless, electrovacuum spacetimes are of great interest, having both a theoretical appeal and exotic astrophysical applications.

In this paper, we initiated an effort toward solving the coupled Einstein-Maxwell equations in a dynamical and fully general relativistic regime. The first step to perform this type of simulations is the generation of valid initial data. Here, we employed the conformal transverse-traceless approach to build a formalism for generating initial data for multiple black holes with charge and angular and linear momenta. Moreover, we applied the theory of isolated horizons to attribute the physical mass, charge, and angular momentum to the horizon, providing a solid understanding of the physical content of our initial data. We implemented the formalism in a software based on the TWO-PUNCTURE

and the `QUASILocalMeasures` open-source codes, verifying our implementation with a series of tests involving analytical or previously known results. The algorithm was found to recover the expected solutions and showed excellent convergence properties.

With the valid initial data for charged, rotating, and moving punctures, it is now possible to simulate dynamical evolution of several systems that have never been taken in consideration, such as ultrarelativistic head-on collision and the quasicircular or eccentric inspiral and merger of two black holes. For a first application of the formalism outlined in this paper, we plan to study in the near future the case of charged and spinning black holes in quasicircular orbit. Some of these simulations are already underway and will be presented in forthcoming work.

ACKNOWLEDGMENTS

We are indebted to the authors of the open-source software that we used: `CACTUS`, `CARPET`, `TWO-PUNCTURES`, `AHFINDER-DIRECT`, and `QUASILocalMeasures`. We thank V. Cardoso, S. Gralla, L. Lehner, U. Sperhake, J. R. Westernacher-Schneider, and M. Zilhão for useful discussions. Computations were performed on the Ocelote cluster at the University of Arizona.

APPENDIX A: ALGORITHM AND IMPORTANT EQUATIONS

In this Appendix, we sketch the algorithm and summarize the important equations to generate initial data for $3 + 1$ evolutions of arbitrary systems of \mathcal{N} black holes with electric charge and linear and angular momenta using the conformal transverse-traceless decomposition. In the following, n is used to index the n th black hole in the system that is $n \in \{1, \dots, \mathcal{N}\}$. Unless otherwise specified, sums in this Appendix are over all punctures. We also assume that each black hole is endowed with Reissner-Nordström electromagnetic fields (\bar{E}^i, \bar{B}^i) associated with electric charge Q_n . The steps in generating the initial data are as follows:

- (1) Choose the bare parameters M_n , Q_n , S_n^i , P_n^i , and \mathbf{x}_n for each black hole, respectively representing mass, charge, angular momentum, linear momentum, and position.
- (2) Compute the conformal electromagnetic fields $(\bar{E}_n^j, \bar{B}_n^j)$ for each black hole. Under the assumption of Reissner-Nordström fields, we obtain

$$\bar{E}_n^j = \frac{Q_n}{R_n^2} \hat{R}_n^j, \quad (\text{A1})$$

$$\bar{B}_n^j = 0, \quad (\text{A2})$$

with $R_n = |\mathbf{x} - \mathbf{x}_n|$ being the Euclidean coordinate distance from puncture n and \hat{R}_n^i being the

corresponding unit vector. Then, superpose the conformal electromagnetic fields of all black holes,

$$\bar{E}^j = \sum \bar{E}_n^j(Q_n, \mathbf{x}_n), \quad (\text{A3})$$

$$\bar{B}^j = \sum \bar{B}_n^j(Q_n, \mathbf{x}_n). \quad (\text{A4})$$

- (3) Solve the inhomogeneous momentum constraint for V_{EM}^i ,

$$(\nabla^2 V_{\text{EM}})^i + \frac{1}{3} \delta^{ij} \partial_j (\partial_k V_{\text{EM}}^k) - 8\pi \bar{S}^i = 0, \quad (\text{A5})$$

with

$$4\pi \bar{S}^i = \bar{\epsilon}^{ijk} \bar{E}_j \bar{B}_k \quad (\text{A6})$$

and imposing as a boundary condition that $V_{\text{EM}}^i \rightarrow 0$ at spatial infinity.

Given our choice for the electromagnetic fields [Eq. (A1)], $\bar{S}^i = 0$, so $V_{\text{EM}} = 0$ is a solution of the momentum constraint (A5).

- (4) Compute the total auxiliary vector V^i ,

$$V^i = V_{\text{GR}}^i + V_{\text{EM}}^i, \quad (\text{A7})$$

with

$$V_{\text{GR}}^i = \sum \left(-\frac{7}{4} \frac{P_n^i}{R_n} - \frac{1}{4} \delta_{jk} x_n^j P_n^k \frac{x_n^i}{R_n^3} + \frac{\bar{\epsilon}_{jk}^i x_n^j S_n^k}{R_n^3} \right). \quad (\text{A8})$$

- (5) Solve the Hamiltonian constraint for u , imposing $u \rightarrow 0$ at spatial infinity,

$$\kappa \nabla^2 u + \partial_a \kappa \partial^a \kappa - \partial_a \varphi \partial^a \varphi - \partial_a \psi \partial^a \psi + \frac{1}{8} \psi^{-6} \bar{A}_{ij} \bar{A}^{ij} + 2\pi \psi^{-2} \bar{\mathcal{E}} = 0, \quad (\text{A9})$$

with

$$\kappa = 1 + u + \eta, \quad (\text{A10})$$

$$\eta = \sum \frac{M_n}{2R_n}, \quad (\text{A11})$$

$$\varphi = \sum \frac{Q_n}{2R_n}, \quad (\text{A12})$$

$$\psi = \sqrt{\kappa^2 - \varphi^2}, \quad (\text{A13})$$

$$\bar{A}_{ij} = 2V_{(i,j)} - \frac{2}{3} \delta_{ij} \partial_k V^k, \quad (\text{A14})$$

$$4\pi\bar{\mathcal{E}} = \frac{1}{2}(\bar{E}_i\bar{E}^i + \bar{B}_i\bar{B}^i). \quad (\text{A15})$$

- (6) With ψ now known, compute the physical fields that are necessary for the evolution:

$$E^i = \psi^{-6}\bar{E}^i, \quad (\text{A16})$$

$$B^i = \psi^{-6}\bar{B}^i, \quad (\text{A17})$$

$$\gamma_{ij} = \psi^4\delta_{ij}, \quad (\text{A18})$$

$$K_{ij} = \psi^{-2}\left(2V_{(i,j)} - \frac{2}{3}\delta_{ij}\partial_k V^k\right). \quad (\text{A19})$$

- (7) Find the isolated horizons \mathcal{S}_n , and compute the associated physical properties

$$Q_{\mathcal{S}_n} = \frac{1}{4\pi} \int_{\mathcal{S}_n} {}^{(4)}\star F, \quad (\text{A20})$$

$$R_{\mathcal{S}_n} = \left(\frac{1}{4\pi} \int_{\mathcal{S}_n} \epsilon\right)^{\frac{1}{2}}, \quad (\text{A21})$$

$$J_{\mathcal{S}_n} = -\frac{1}{8\pi} \int_{\mathcal{S}_n} (\varphi \cdot \omega)\epsilon + 2(\varphi \cdot {}^{(4)}A){}^{(4)}\star F, \quad (\text{A22})$$

$$M_{\mathcal{S}_n} = \frac{1}{2R_{\mathcal{S}_n}} [(R_{\mathcal{S}_n}^2 + Q_{\mathcal{S}_n}^2)^2 + 4J_{\mathcal{S}_n}^2]^{\frac{1}{2}}, \quad (\text{A23})$$

where ${}^{(4)}\star F$ is the dual of the electromagnetic tensor, ϵ is the horizon surface 2-form, ${}^{(4)}A$ is the electromagnetic vector potential, φ is the approximate rotational Killing vector on \mathcal{S}_n , and ω is defined in the main text [see Eq. (24)]. $Q_{\mathcal{S}_n}$, $R_{\mathcal{S}_n}$, $J_{\mathcal{S}_n}$, and $M_{\mathcal{S}_n}$ are, respectively, the charge, radius, angular momentum, and mass of the n th horizon.

APPENDIX B: ISOLATED HORIZON IN THE REISSNER-NORDSTRÖM SOLUTION

The goal of this Appendix is to show that the formalism of isolated horizons produces the expected black hole properties in the case of the Reissner-Nordström solution. This can be proven starting from metric (17), which we rewrite here for convenience,

$$ds^2 = -\left(1 - \frac{2m}{r} + \frac{q}{r^2}\right)dt^2 + \left(1 - \frac{2m}{r} + \frac{q}{r^2}\right)^{-1}dr^2 + r^2(d\theta^2 + \sin^2\theta d\phi^2), \quad (\text{B1})$$

with electromagnetic potential

$${}^{(4)}A = -\frac{q}{r}dt. \quad (\text{B2})$$

In this case, a spherical surface with coordinate radius $r_+ = m + \sqrt{m^2 - q^2}$ is a Killing horizon, which implies that it is an isolated horizon. This is because every Killing horizon which is topologically $S^2 \times \mathbb{R}$ is an isolated horizon [93]. Therefore, the metric \mathfrak{q}_{ab} induced on the spatial section of the horizon is simply the metric on a spherical surface [$ds^2 = \mathfrak{q}_{ab}dx^a dx^b = r^2(d\theta^2 + \sin^2\theta d\phi^2)$], and the value of $R_{\mathcal{S}}$ defined by Eq. (23) coincides with r_+ itself, since the radial coordinate in Eq. (B1) is the areal radius. In this case, the rotational vector φ in (24) is taken to be the generator of the azimuthal symmetry on the sphere, which is also a Killing vector of the entire spacetime. Hence, we find that $\varphi \cdot {}^{(4)}A = 0$ as ${}^{(4)}A$ has only a temporal component and φ has only a spatial component. Moreover, since the future-directed vector k^a orthogonal to \mathcal{S} has only radial and temporal components, and any t^a tangent to \mathcal{S} has only azimuthal and meridional components, $t^a \nabla_a k^b = 0$. By construction, we also have $t^a \nabla_a k^b = t^a \omega_a k^b = 0$, which implies that $\omega_a = 0$, because the equation is zero for each t^a . Hence, by use of Eq. (24), we conclude that $J_{\mathcal{S}} = 0$.

To compute charge and mass, we need the electromagnetic tensor, which is given by

$${}^{(4)}F = d{}^{(4)}A = -\frac{q}{r^2}dr \wedge dt = \frac{q}{r^2}dt \wedge dr, \quad (\text{B3})$$

and its dual

$${}^{(4)}\star F = \sqrt{-g} \frac{q}{r^2} d\theta \wedge d\phi = q \sin\theta d\theta \wedge d\phi. \quad (\text{B4})$$

The integration of ${}^{(4)}\star F/4\pi$ over any sphere of coordinate radius r results in exactly q , so Eq. (25) implies $Q_{\mathcal{S}} = q$.

Finally, from Eq. (26), the horizon mass is

$$M_{\mathcal{S}} = \frac{(R_{\mathcal{S}}^2 + q^2)}{2R_{\mathcal{S}}} = \frac{2m(m + \sqrt{m^2 - q^2})}{2(m + \sqrt{m^2 - q^2})} = m. \quad (\text{B5})$$

For a Reissner-Nordström black hole, m and q are interpreted as the spacetime total energy and electric charge, respectively [59]. Therefore, in this case, the bare mass (charge), the isolated horizon mass (charge), and the physical mass (charge) all coincide.

APPENDIX C: COMPUTING THE CHARGE OF AN ISOLATED HORIZON

In this Appendix, we discuss how we perform the computation of the horizon charge. To compute the charge of the horizon, we need to perform the following integration (see Sec. II C):

$$Q_S = \frac{1}{4\pi} \int_S \frac{1}{2!} \epsilon_{abc} E^c dx^a \wedge dx^b. \quad (\text{C1})$$

This quantity is coordinate independent, so choosing Cartesian coordinates $(x^a) = (x, y, z)$, we can write

$$Q_S = \frac{1}{4\pi} \int_S \sqrt{\gamma} (E_z dx \wedge dy + E_x dy \wedge dz - E_y dx \wedge dz), \quad (\text{C2})$$

with γ being the determinant of the spatial metric. We introduce a parametrization of S with polar coordinates (θ, ϕ) around the origin (x_0, y_0, z_0) ,

$$\begin{cases} x(\theta, \phi) = x_0 + s(\theta, \phi) \sin \theta \cos \phi \\ y(\theta, \phi) = y_0 + s(\theta, \phi) \sin \theta \sin \phi, \\ z(\theta, \phi) = z_0 + s(\theta, \phi) \cos \theta \end{cases} \quad (\text{C3})$$

with $s(\theta, \phi)$ being suitable smooth function. This is always possible since by hypothesis S has spherical topology and by construction Q_S does not depend on the parametrization. Then, the first term in Eq. (C2) can be written as

$$\begin{aligned} & \int_S \sqrt{\gamma} E_z(x, y, z) dx \wedge dy \\ &= \int_\theta \int_\phi \sqrt{\gamma} E_z(\theta, \phi) |\det J_{xy}(\theta, \phi)| d\theta d\phi, \end{aligned} \quad (\text{C4})$$

where $J_{xy}(\theta, \phi)$ is the Jacobian of the transformation (C3) involving the coordinates x and y ,

$$J_{xy}(\theta, \phi) = \begin{pmatrix} \partial_\theta x(\theta, \phi) & \partial_\phi x(\theta, \phi) \\ \partial_\theta y(\theta, \phi) & \partial_\phi y(\theta, \phi) \end{pmatrix}.$$

The remaining terms in Eq. (C2) are dealt with accordingly.

In QUASILocalMEASURESEM, we use the parametrization $s(\theta, \phi)$ provided by AHFINDERDIRECT, and we compute the derivatives in the Jacobians using a centered, second-order accurate finite-difference scheme.

APPENDIX D: KERR-NEWMAN SPACETIME

In this Appendix, we review the Kerr-Newman spacetime and discuss challenges associated with using the Kerr-Newman electromagnetic fields as source terms in the Hamiltonian and momentum constraints.

The Kerr-Newman black hole with mass m , electric charge q , and angular momentum am in Boyer-Lindquist coordinates (t, r, θ, ϕ) is [59]

$$\begin{aligned} ds^2 = & -\frac{\Delta - a^2 \sin^2 \theta}{\rho^2} dt^2 + \frac{\rho^2}{\Delta} dr^2 + \rho^2 d\theta^2 \\ & - 2a \sin^2 \theta \frac{(r^2 + a^2 - \Delta)}{\rho^2} dt d\phi \\ & + \frac{(r^2 + a^2)^2 - \Delta a^2 \sin^2 \theta}{\rho^2} \sin^2 \theta d\phi^2, \end{aligned} \quad (\text{D1})$$

with

$$\rho^2 = r^2 + a^2 \cos^2 \theta, \quad (\text{D2a})$$

$$\Delta = r^2 - 2mr + a^2 + q^2. \quad (\text{D2b})$$

The electromagnetic vector potential is

$${}^{(4)}A = -\frac{qr}{\rho^2} (dt - a \sin^2 \theta d\phi). \quad (\text{D3})$$

Following the usual procedure for generating puncture initial data, we transform to quasi-isotropic coordinates by introducing a new radial coordinate R as in Ref. [90]

$$r = R \left(1 + \frac{m}{R} + \frac{R_H^2}{R^2} \right), \quad (\text{D4})$$

with $R_H = \frac{1}{2} \sqrt{m^2 - a^2 - q^2}$ being the radius of the black hole horizon in the new coordinate system. The metric takes now the form

$$ds^2 = (-\alpha^2 + \beta_\phi \beta^\phi) dt^2 + 2\beta_\phi d\phi dt + \gamma_{lk} dx^l dx^k, \quad (\text{D5})$$

where

$$\begin{aligned} \gamma_{lk} dx^l dx^k = & \Psi^4 [dR^2 + R^2 d\theta^2 + R^2 \sin^2 \theta d\phi^2 \\ & \times a^2 h R^4 \sin^4 \theta d\phi^2], \end{aligned} \quad (\text{D6})$$

where Ψ is the conformal factor; $l, k \in \{R, \theta, \phi\}$; and α, β, γ , and h are functions of (R, θ, ϕ) , with

$$\Psi^4 = \rho^2 / R^2, \quad (\text{D7a})$$

$$\alpha = \frac{\rho^6 (R + R_H)(R - R_H)}{R\Upsilon}, \quad (\text{D7b})$$

$$\beta_\phi = -a\sigma \sin^2 \theta, \quad (\text{D7c})$$

$$\beta^\phi = \beta_\phi / \gamma_{\phi\phi}, \quad (\text{D7d})$$

$$h = (1 + \sigma) / (\rho^2 R^2), \quad (\text{D7e})$$

$$\sigma = \frac{2mr - q^2}{\rho^2}, \quad (\text{D7f})$$

$$\Upsilon = \rho^6 \sqrt{r^2 + a^2(1 + \sigma \sin^2 \theta)}, \quad (\text{D7g})$$

$$\gamma_{\phi\phi} = \sin^2 \theta (r^2 + a^2(1 + \sigma \sin^2 \theta)). \quad (\text{D7h})$$

The nonzero components of the electromagnetic fields are⁸

$$E^R = \frac{qR(2r^2 - \rho^2)(r^2 + a^2)}{\Upsilon}, \quad (\text{D8a})$$

$$E^\theta = -\frac{2a^2q(R - R_H)(R + R_H)r \cos \theta \sin \theta}{R\Upsilon}, \quad (\text{D8b})$$

$$B^R = \frac{2aqRr(r^2 + a^2) \cos \theta}{\Upsilon}, \quad (\text{D8c})$$

$$B^\theta = \frac{aq(R - R_H)(R + R_H)(2r^2 - \rho^2) \sin \theta}{R\Upsilon}. \quad (\text{D8d})$$

The conformal fields are obtained by scaling by $\sqrt{\Upsilon} = \Upsilon \rho^{-4} R^{-1} \sin \theta$,

$$\bar{E}^R = \frac{q(2r^2 - \rho^2)(r^2 + a^2) \sin \theta}{\rho^4}, \quad (\text{D9a})$$

$$\bar{E}^\theta = -\frac{2a^2q(R - R_H)(R + R_H)r \cos \theta \sin^2 \theta}{\rho^4 R^2}, \quad (\text{D9b})$$

$$\bar{B}^R = \frac{2aqr(r^2 + a^2) \cos \theta \sin \theta}{\rho^4}, \quad (\text{D9c})$$

$$\bar{B}^\theta = \frac{aq(R - R_H)(R + R_H)(2r^2 - \rho^2) \sin^2 \theta}{\rho^4 R^2}. \quad (\text{D9d})$$

In these coordinates, the conformal fields are regular for $R \rightarrow 0$ (in this limit, $\rho \sim r \sim 1/R$).

However, Eqs. (46) and (50) are in Cartesian coordinates. Transforming to Cartesian coordinates as in flat spacetime, the conformal fields are obtained as

$$\bar{E}^i = \frac{\partial x^i}{\partial R} \frac{\bar{E}^R}{R^2 \sin \theta} + \frac{\partial x^i}{\partial \theta} \frac{\bar{E}^\theta}{R^2 \sin \theta}, \quad (\text{D10a})$$

⁸Our expression for E^θ differs from the corresponding one in Eq. (3.5) of Ref. [90] by a factor of r/R . We find that the electric-field components listed in Ref. [90] do not satisfy Maxwell's equations and that Gauss's law yields a value for the charge that is correct for spherical surfaces, but the value is different on nonspherical surfaces, e.g., ellipsoidal ones. We have checked that our electric fields satisfy Maxwell's equations, and as a result, Gauss's law yields the correct electric charge even on nonspherical surfaces. We conclude that E^θ in Ref. [90] has a typographical error.

$$\bar{B}^i = \frac{\partial x^i}{\partial R} \frac{\bar{B}^R}{R^2 \sin \theta} + \frac{\partial x^i}{\partial \theta} \frac{\bar{B}^\theta}{R^2 \sin \theta}, \quad (\text{D10b})$$

where here $i \in \{x, y, z\}$ and the factor of $R^2 \sin \theta$ is the determinant of the Jacobian of the transformation and ensures that the resulting fields \bar{E}^i and \bar{B}^i satisfy the Maxwell constraints

$$\partial_i \bar{E}^i = 0, \quad (\text{D11a})$$

$$\partial_i \bar{B}^i = 0. \quad (\text{D11b})$$

In these coordinates, the fields are singular when $x, y, z \rightarrow 0$. Given this singular behavior, V_{EM}^i is expected to be singular as well near the punctures because the source of the momentum constraint (46) diverges with a high power of R . This is precisely what we find when we implement our algorithm with the Kerr-Newman electromagnetic fields. In particular, for a single Kerr-Newman black hole without linear momentum, the singular source terms are \bar{S}^x and \bar{S}^y , which at leading order for $x, y, z \rightarrow 0$ scale as

$$\bar{S}^x \sim \frac{aq^2 y}{R_H (x^2 + y^2 + z^2)^{\frac{5}{2}}}, \quad (\text{D12a})$$

$$\bar{S}^y \sim -\frac{aq^2 x}{R_H (x^2 + y^2 + z^2)^{\frac{5}{2}}}. \quad (\text{D12b})$$

A possible approach to dealing with the singular source would be to separate the singular part of the solution from the regular one, as is done for the Hamiltonian constraint. However, this approach typically requires a known analytic solution, and this does not seem possible within the approach of conformal flatness because the Kerr-Newman solution does not admit conformally flat spatial slices. In future work, we will explore potential solutions to these challenges by lifting the conformal flatness approximation.

APPENDIX E: GENERALIZED MAJUMDAR-PAPAPETROU

Here, we show that our formalism recovers spatial slices of a generalized Majumdar-Papapetrou solution found by Ref. [86] when each black hole is at rest and nonspinning and all black holes have the same charge-to-mass ratio. This happens because under these assumptions the momentum constraint is trivially satisfied, and the Hamiltonian one is solved by $u = 0$, as we verify in what follows.

Given our definitions of η and φ [Eqs. (48)], if the charge-to-mass ratio is fixed to λ for every black hole, then $\varphi = \lambda\eta$. Moreover, with our choice of Reissner-Nordström fields, there are no magnetic fields, so the electromagnetic energy is $8\pi\bar{\mathcal{E}} = 4\partial_a \varphi \partial^a \varphi$, where the factor of 4 arises

from the fact that φ is not the electrostatic potential, but it is *half* of it. Plugging the ansatz $u = 0$ into the Hamiltonian constraint [Eq. (50)] yields

$$\partial_a \kappa \partial^a \kappa - \partial_a \varphi \partial^a \varphi - \partial_a \psi \partial^a \psi + \psi^{-2} \partial_a \varphi \partial^a \varphi = 0. \quad (\text{E1})$$

But $\psi = \sqrt{\kappa^2 - \varphi^2}$; thus, multiplying the last equation by ψ^2 and expressing the derivatives of ψ in terms of κ and φ and their derivatives yields

$$(1 - \kappa^2) \partial_a \varphi \partial^a \varphi - \varphi^2 \partial_a \kappa \partial^a \kappa + 2\kappa \varphi \partial_a \kappa \partial^a \varphi = 0. \quad (\text{E2})$$

Plugging $\kappa = 1 + \eta = 1 + \varphi/\lambda$ and $\partial_a \kappa = \partial_a \varphi/\lambda$ into this last expression, after some algebra, we find that the Hamiltonian constraint is satisfied. If we choose $\lambda = 1$, we find

$$\gamma_{ij} = \left(1 + \sum_{n=1}^{N_p} \frac{M_n}{R_n}\right) \delta_{ij}, \quad (\text{E3})$$

which describes a spatial slice of the Majumdar-Papapetrou spacetime with N extremal black holes [54,55].

-
- [1] B. P. Abbott, R. Abbott, T. D. Abbott, M. R. Abernathy, F. Acernese, K. Ackley, C. Adams, T. Adams, P. Addesso, R. X. Adhikari *et al.*, *Phys. Rev. Lett.* **116**, 131103 (2016).
- [2] B. P. Abbott, R. Abbott, T. D. Abbott, M. R. Abernathy, F. Acernese, K. Ackley, C. Adams, T. Adams, P. Addesso, R. X. Adhikari *et al.*, *Phys. Rev. Lett.* **116**, 241103 (2016).
- [3] B. P. Abbott, R. Abbott, T. D. Abbott, F. Acernese, K. Ackley, C. Adams, T. Adams, P. Addesso, R. X. Adhikari, V. B. Adya *et al.*, *Phys. Rev. Lett.* **118**, 221101 (2017).
- [4] B. P. Abbott, R. Abbott, T. D. Abbott, F. Acernese, K. Ackley, C. Adams, T. Adams, P. Addesso, R. X. Adhikari, and V. B. Adya, *Phys. Rev. Lett.* **119**, 141101 (2017).
- [5] LIGO Scientific and Virgo Collaborations, [arXiv:1811.12907](https://arxiv.org/abs/1811.12907).
- [6] É. É. Flanagan and S. A. Hughes, *Phys. Rev. D* **57**, 4535 (1998).
- [7] É. É. Flanagan and S. A. Hughes, *Phys. Rev. D* **57**, 4566 (1998).
- [8] B. Aylott, J. G. Baker, W. D. Boggs, M. Boyle, P. R. Brady, D. A. Brown, B. Brügmann, L. T. Buchman, A. Buonanno, L. Cadonati, J. Camp, M. Campanelli, J. Centrella, S. Chatterji, N. Christensen, T. Chu, P. Diener, N. Dorband, Z. B. Etienne *et al.*, *Classical Quantum Gravity* **26**, 165008 (2009).
- [9] P. Ajith, M. Boyle, D. A. Brown, B. Brügmann, L. T. Buchman, L. Cadonati, M. Campanelli, T. Chu, Z. B. Etienne, S. Fairhurst, M. Hannam, J. Healy, I. Hinder, S. Husa *et al.*, *Classical Quantum Gravity* **29**, 124001 (2012).
- [10] I. Hinder *et al.*, *Classical Quantum Gravity* **31**, 025012 (2014).
- [11] F. Pretorius, *Phys. Rev. Lett.* **95**, 121101 (2005).
- [12] M. Campanelli, C. O. Lousto, P. Marronetti, and Y. Zlochower, *Phys. Rev. Lett.* **96**, 111101 (2006).
- [13] J. G. Baker, J. Centrella, D.-I. Choi, M. Koppitz, and J. van Meter, *Phys. Rev. Lett.* **96**, 111102 (2006).
- [14] A. Gopakumar, M. Hannam, S. Husa, and B. Brügmann, *Phys. Rev. D* **78**, 064026 (2008).
- [15] G. Lovelace, M. Boyle, M. A. Scheel, and B. Szilágyi, *Classical Quantum Gravity* **29**, 045003 (2012).
- [16] T. Chu, H. Fong, P. Kumar, H. P. Pfeiffer, M. Boyle, D. A. Hemberger, L. E. Kidder, M. A. Scheel, and B. Szilágyi, *Classical Quantum Gravity* **33**, 165001 (2016).
- [17] G. Lovelace *et al.*, *Classical Quantum Gravity* **33**, 244002 (2016).
- [18] K. Jani, J. Healy, J. A. Clark, L. London, P. Laguna, and D. Shoemaker, *Classical Quantum Gravity* **33**, 204001 (2016).
- [19] J. Healy, C. O. Lousto, Y. Zlochower, and M. Campanelli, *Classical Quantum Gravity* **34**, 224001 (2017).
- [20] J. Healy, C. O. Lousto, J. Lange, R. O’Shaughnessy, Y. Zlochower, and M. Campanelli, [arXiv:1901.02553](https://arxiv.org/abs/1901.02553).
- [21] T. Baumgarte, P. R. Brady, J. D. E. Creighton, L. Lehner, F. Pretorius, and R. Devoe, *Phys. Rev. D* **77**, 084009 (2008).
- [22] M. A. Scheel, M. Boyle, T. Chu, L. E. Kidder, K. D. Matthews, and H. P. Pfeiffer, *Phys. Rev. D* **79**, 024003 (2009).
- [23] J. Lange *et al.*, *Phys. Rev. D* **96**, 104041 (2017).
- [24] T. W. Baumgarte and S. L. Shapiro, *Numerical Relativity: Solving Einstein’s Equations on the Computer* (Cambridge University Press, Cambridge, England, 2010).
- [25] B. P. Abbott, R. Abbott, T. D. Abbott, F. Acernese, K. Ackley, C. Adams, T. Adams, P. Addesso, R. X. Adhikari, V. B. Adya *et al.* (LIGO Scientific and Virgo Collaborations), *Phys. Rev. Lett.* **119**, 161101 (2017).
- [26] H. Yang, W. E. East, and L. Lehner, *Astrophys. J.* **856**, 110 (2018).
- [27] T. Hinderer *et al.*, [arXiv:1808.03836](https://arxiv.org/abs/1808.03836).
- [28] F. Foucart, T. Hinderer, and S. Nissanke, *Phys. Rev. D* **98**, 081501 (2018).
- [29] M. W. Coughlin and T. Dietrich, [arXiv:1901.06052](https://arxiv.org/abs/1901.06052).
- [30] J. A. Font, *Living Rev. Relativity* **11**, 7 (2008).
- [31] Z. B. Etienne, Y. T. Liu, V. Paschalidis, and S. L. Shapiro, *Phys. Rev. D* **85**, 064029 (2012).
- [32] M. Shibata and K. Taniguchi, *Living Rev. Relativity* **14**, 6 (2011).
- [33] J. A. Faber and F. A. Rasio, *Living Rev. Relativity* **15**, 8 (2012).
- [34] L. Lehner and F. Pretorius, *Annu. Rev. Astron. Astrophys.* **52**, 661 (2014).

- [35] V. Paschalidis, *Classical Quantum Gravity* **34**, 084002 (2017).
- [36] V. Paschalidis and N. Stergioulas, *Living Rev. Relativity* **20**, 7 (2017).
- [37] L. Baiotti and L. Rezzolla, *Rep. Prog. Phys.* **80**, 096901 (2017).
- [38] M. D. Duez and Y. Zlochower, *Rep. Prog. Phys.* **82**, 016902 (2019).
- [39] V. Cardoso *et al.*, *Classical Quantum Gravity* **29**, 244001 (2012).
- [40] C. Palenzuela, L. Lehner, and S. L. Liebling, *Science* **329**, 927 (2010).
- [41] L. Lehner, C. Palenzuela, S. L. Liebling, C. Thompson, and C. Hanna, *Phys. Rev. D* **86**, 104035 (2012).
- [42] P. Moesta, D. Alic, L. Rezzolla, O. Zanotti, and C. Palenzuela, *Astrophys. J. Lett.* **749**, L32 (2012).
- [43] D. Alic, P. Moesta, L. Rezzolla, O. Zanotti, and J. L. Jaramillo, *Astrophys. J.* **754**, 36 (2012).
- [44] V. Paschalidis and S. L. Shapiro, *Phys. Rev. D* **88**, 104031 (2013).
- [45] V. Paschalidis, Z. B. Etienne, and S. L. Shapiro, *Phys. Rev. D* **88**, 021504 (2013).
- [46] M. Ponce, C. Palenzuela, L. Lehner, and S. L. Liebling, *Phys. Rev. D* **90**, 044007 (2014).
- [47] W. E. East and H. Yang, *Phys. Rev. D* **98**, 023008 (2018).
- [48] T. Kaluza, *Sitzungsberichte der Königlich Preußischen Akademie der Wissenschaften (Berlin)* **34**, 966 (1921).
- [49] O. Klein, *Z. Phys.* **37**, 895 (1926).
- [50] H. Reissner, *Ann. Phys. (N.Y.)* **355**, 106 (1916).
- [51] G. Nordström, *Proc. K. Ned. Akad. Wet., Ser. B* **20**, 1238 (1918).
- [52] E. T. Newman, E. Couch, K. Chinnapared, A. Exton, A. Prakash, and R. Torrence, *J. Math. Phys. (N.Y.)* **6**, 918 (1965).
- [53] R. P. Kerr, *Phys. Rev. Lett.* **11**, 237 (1963).
- [54] S. D. Majumdar, *Phys. Rev.* **72**, 390 (1947).
- [55] A. Papapetrou, *Proc. R. Ir. Acad. Sect. A* **51**, 191 (1945).
- [56] Z. Perjés, *Phys. Rev. Lett.* **27**, 1668 (1971).
- [57] W. Israel and G. A. Wilson, *J. Math. Phys. (N.Y.)* **13**, 865 (1972).
- [58] J. B. Hartle and S. W. Hawking, *Commun. Math. Phys.* **26**, 87 (1972).
- [59] R. M. Wald, *General Relativity* (University of Chicago, Chicago, 1984).
- [60] G. W. Gibbons, *Commun. Math. Phys.* **44**, 245 (1975).
- [61] R. M. Wald, *Phys. Rev. D* **10**, 1680 (1974).
- [62] A. Eckart, M. García-Marín, S. N. Vogel, P. Teuben, M. R. Morris, F. Baganoff, J. Dexter, R. Schödel, G. Witzel, M. Valencia-S., V. Karas, D. Kunneriath, C. Straubmeier, L. Moser, N. Sabha, R. Buchholz, M. Zamaninasab, K. Mužić, J. Moutlaka, and J. A. Zensus, *Astron. Astrophys.* **537**, A52 (2012).
- [63] R. P. Eatough *et al.*, *Nature (London)* **501**, 391 (2013).
- [64] J. Levin, D. J. D’Orazio, and S. Garcia-Saenz, *Phys. Rev. D* **98**, 123002 (2018).
- [65] S. Ray, A. L. Espíndola, M. Malheiro, J. P. Lemos, and V. T. Zanchin, *Phys. Rev. D* **68**, 084004 (2003).
- [66] A. Nathanail, E. R. Most, and L. Rezzolla, *Mon. Not. R. Astron. Soc.* **469**, L31 (2017).
- [67] T. Liu, G. E. Romero, M.-L. Liu, and A. Li, *Astrophys. J.* **826**, 82 (2016).
- [68] V. Cardoso, C. F. B. Macedo, P. Pani, and V. Ferrari, *J. Cosmol. Astropart. Phys.* **05** (2016) 054.
- [69] U. Sperhake, V. Cardoso, F. Pretorius, E. Berti, and J. A. González, *Phys. Rev. Lett.* **101**, 161101 (2008).
- [70] U. Sperhake, V. Cardoso, F. Pretorius, E. Berti, T. Hinderer, and N. Yunes, *Phys. Rev. Lett.* **103**, 131102 (2009).
- [71] E. Berti, V. Cardoso, T. Hinderer, M. Lemos, F. Pretorius, U. Sperhake, and N. Yunes, *Phys. Rev. D* **81**, 104048 (2010).
- [72] U. Sperhake, E. Berti, V. Cardoso, and F. Pretorius, *Phys. Rev. Lett.* **111**, 041101 (2013).
- [73] Y. Mo, Y. Tian, B. Wang, H. Zhang, and Z. Zhong, *Phys. Rev. D* **98**, 124025 (2018).
- [74] O. J. C. Dias, H. S. Reall, and J. E. Santos, *Classical Quantum Gravity* **36**, 045005 (2019).
- [75] O. J. C. Dias, F. C. Eperon, H. S. Reall, and J. E. Santos, *Phys. Rev. D* **97**, 104060 (2018).
- [76] V. Cardoso, J. L. Costa, K. Destounis, P. Hintz, and A. Jansen, *Phys. Rev. D* **98**, 104007 (2018).
- [77] B. Zhang, *Astrophys. J. Lett.* **827**, L31 (2016).
- [78] B. P. Abbott *et al.* (LIGO Scientific and Virgo Collaborations), *Phys. Rev. Lett.* **116**, 061102 (2016).
- [79] V. Connaughton *et al.*, *Astrophys. J. Lett.* **826**, L6 (2016).
- [80] F. Fraschetti, *J. Cosmol. Astropart. Phys.* **4** (2018) 054.
- [81] S. L. Liebling and C. Palenzuela, *Phys. Rev. D* **94**, 064046 (2016).
- [82] R. L. Arnowitt, S. Deser, and C. W. Misner, *Gen. Relativ. Gravit.* **40**, 1997 (2008).
- [83] J. W. York, *Phys. Rev. Lett.* **26**, 1656 (1971).
- [84] F. Pretorius, *Classical Quantum Gravity* **22**, 425 (2005).
- [85] K. S. Thorne and D. MacDonald, *Mon. Not. R. Astron. Soc.* **198**, 339 (1982).
- [86] M. Alcubierre, J. C. Degollado, and M. Salgado, *Phys. Rev. D* **80**, 104022 (2009).
- [87] J. M. Bowen, *Ann. Phys. (N.Y.)* **165**, 17 (1985).
- [88] M. Zilhão, V. Cardoso, C. Herdeiro, L. Lehner, and U. Sperhake, *Phys. Rev. D* **85**, 124062 (2012).
- [89] M. Zilhão, V. Cardoso, C. Herdeiro, L. Lehner, and U. Sperhake, *Phys. Rev. D* **89**, 044008 (2014).
- [90] M. Zilhão, V. Cardoso, C. Herdeiro, L. Lehner, and U. Sperhake, *Phys. Rev. D* **90**, 124088 (2014).
- [91] J. M. Bowen and J. W. York, Jr., *Phys. Rev. D* **21**, 2047 (1980).
- [92] M. Ansorg, B. Brügmann, and W. Tichy, *Phys. Rev. D* **70**, 064011 (2004).
- [93] A. Ashtekar, C. Beetle, O. Dreyer, S. Fairhurst, B. Krishnan, J. Lewandowski, and J. Wiśniewski, *Phys. Rev. Lett.* **85**, 3564 (2000).
- [94] O. Dreyer, B. Krishnan, D. Shoemaker, and E. Schnetter, *Phys. Rev. D* **67**, 024018 (2003).
- [95] C. W. Misner, K. S. Thorne, and J. A. Wheeler, *General Relativity* (Freeman, San Francisco, 1973).
- [96] J. D. Jackson, *Classical Electrodynamics* (Wiley, New York, 1975).
- [97] T. W. Baumgarte and S. L. Shapiro, *Numerical Relativity: Solving Einstein’s Equations on the Computer* (Cambridge University Press, Cambridge, England, 2010).

- [98] R. Arnowitt, S. Deser, and C. W. Misner, *Gen. Relativ. Gravit.* **40**, 1997 (2008).
- [99] T. W. Baumgarte and S. L. Shapiro, *Astrophys. J.* **585**, 921 (2003).
- [100] A. Ashtekar and B. Krishnan, *Living Rev. Relativity* **7**, 10 (2004).
- [101] E. Schnetter, B. Krishnan, and F. Beyer, *Phys. Rev. D* **74**, 024028 (2006).
- [102] R. Penrose, *Phys. Rev. Lett.* **14**, 57 (1965).
- [103] S. W. Hawking and R. Penrose, *Proc. R. Soc. Ser. A* **314**, 529 (1970).
- [104] B. Krishnan, *Isolated Horizons in Numerical Relativity*, Ph.D. thesis, Pennsylvania State University, 2002.
- [105] A. Ashtekar, C. Beetle, and J. Lewandowski, *Phys. Rev. D* **64**, 044016 (2001).
- [106] L. Del Zanna, N. Bucciantini, and P. Londrillo, *Astron. Astrophys.* **400**, 397 (2003).
- [107] B. Giacomazzo, L. Rezzolla, and L. Baiotti, *Phys. Rev. D* **83**, 044014 (2011).
- [108] Z. B. Etienne, V. Paschalidis, Y. T. Liu, and S. L. Shapiro, *Phys. Rev. D* **85**, 024013 (2012).
- [109] Z. B. Etienne, V. Paschalidis, R. Haas, P. Msta, and S. L. Shapiro, *Classical Quantum Gravity* **32**, 175009 (2015).
- [110] P. C. Fragile, D. Nemergut, P. L. Shaw, and P. Anninos, [arXiv:1812.01701](https://arxiv.org/abs/1812.01701).
- [111] G. B. Cook, *Living Rev. Relativity* **3**, 5 (2000).
- [112] C. O. Lousto, H. Nakano, Y. Zlochower, B. C. Mundim, and M. Campanelli, *Phys. Rev. D* **85**, 124013 (2012).
- [113] A. Garat and R. H. Price, *Phys. Rev. D* **61**, 124011 (2000).
- [114] S. R. Brandt and E. Seidel, *Phys. Rev. D* **52**, 870 (1995).
- [115] R. J. Gleiser, C. O. Nicasio, R. H. Price, and J. Pullin, *Phys. Rev. D* **57**, 3401 (1998).
- [116] L. Smarr and J. W. York, Jr., *Phys. Rev. D* **17**, 2529 (1978).
- [117] S. Brandt and B. Brügmann, *Phys. Rev. Lett.* **78**, 3606 (1997).
- [118] T. Goodale, G. Allen, G. Lanfermann, J. Massó, T. Radke, E. Seidel, and J. Shalf, *Vector and parallel processing—VECPAR'2002*, in *Proceedings of the 5th International Conference*, Lecture Notes in Computer Science (Springer, Berlin, 2003).
- [119] E. Schnetter, S. H. Hawley, and I. Hawke, *Classical Quantum Gravity* **21**, 1465 (2004).
- [120] V. Paschalidis, Z. B. Etienne, R. Gold, and S. L. Shapiro, [arXiv:1304.0457](https://arxiv.org/abs/1304.0457).
- [121] J. Thornburg, *Classical Quantum Gravity* **21**, 743 (2004).
- [122] R. Barrett, M. Berry, T. F. Chan, J. Demmel, J. Donato, J. Dongarra, V. Eijkhout, R. Pozo, C. Romine, and H. V. der Vorst, *Templates for the Solution of Linear Systems: Building Blocks for Iterative Methods*, 2nd ed. (SIAM, Philadelphia, 1994).
- [123] K. A. Dennison, T. W. Baumgarte, and H. P. Pfeiffer, *Phys. Rev. D* **74**, 064016 (2006).